The University of Queensland

Bachelor of Engineering Thesis

Performance Evaluation of an Implicitly-Regularised Model for Viscoplastic Particle Suspensions

Student Name: Nathan J. DI VAIRA

Course Code: MECH4500

Supervisor: Dr. Christopher R. Leonardi

Submission Date: 28th October 2016

A thesis submitted in partial fulfilment of the requirements of the Bachelor of Engineering Degree in Mechanical Engineering

UQ Engineering

Faculty of Engineering, Architecture and Information Technology

Acknowledgements

Firstly, I would like to show my appreciation towards my supervisor, Dr. Christopher Leonardi, for all of the support and advice over the last six months. Your thorough feedback and constant interest in and dedication to the project drove me to produce the highest quality work I could. My development throughout the project has been immeasurable, with the work opening my eyes to a world of future career possibilities, and for those things I am grateful.

To Wojciech Regulski in Poland, thank you for the many code implementations, constant assistance, and the opportunity to share in your work. This was as much your project as it was mine. Good luck with your current work and future studies.

Finally, to my family, thank you for keeping me grounded and providing an unwavering source of support that I could depend upon. To my friends, thank you for the much needed laughter (even if it did verge on hysterical at times) and for providing numerous outlets for me to blow off some steam. This year has been the most challenging of my life so far, but also the most enjoyable.

Abstract

Due to their unique properties, dense viscoplastic fluid-particle suspensions have significant potential to be used in a number of industrial applications, from hydraulic fracturing to pipeline particulate transport. However, the rheological properties of these suspensions are currently poorly understood, with no comprehensive modelling strategies existing to predict their behaviour. Numerous numerical difficulties arise when attempting to model viscoplastic suspensions, a key cause of which is the presence of a fluid yield-stress. Currently, a number of explicit regularisation techniques are used to approximate the yield-stress, the inherent numerical inaccuracies of which are quite often given little attention.

A coupled LBM-DEM numerical approach presents an excellent solution to modelling the bulk movement of particles within suspensions, and has been successfully applied to the modelling of dense Newtonian suspensions. Of key importance, however, the LBM allows for an implicit regularisation of the yield-stress, in which the constitutive Bingham fluid is solved without the need for the approximations of current explicit solvers. Hence, it was hypothesised that the implicitly-regularised (IR) model is superior for the modelling of viscoplastic fluids, a claim which, if true, would lead to the eventual direct numerical simulation of dense viscoplastic particle suspensions. Consequently, the aim of the investigation was to evaluate the performance of the IR LBM-DEM in viscoplastic fluid-particle coupling, compared to that of the explicit Papanastasiou-regularised (PR) two-relaxation-time (TRT) method.

To achieve this, five numerical testing models were developed, based off existing numerical and experimental studies of simplified benchmark problems in the literature. These 2-D and 3-D simulations provided a basis for the validation of the IR model, as well as a means for performance comparisons between the IR and TRT models.

In initial 2-D simulations, the TRT model exhibited a narrow range of numerical stability and highly viscosity-dependent behaviour in Bingham fluids, evidencing the conclusion that the ill-defined PR constitutive model manifested numerical inaccuracies when coupled with the kinetic nature of the LBM. By comparison, a wide range of numerical stability was observed in the implicitly-regularised results, as well as minimal dependence on the fluid viscosity, with results closely matching those from the literature. For the 3-D tests, the IR model exhibited excellent qualitative and quantitative agreement with literature

results in both the creeping and inertial regimes, proving the successful modelling of yield-stress, viscous and inertial effects on particle behaviour. While the TRT model showed reasonable correlation to the literature, drag was consistently under-predicted, suggesting that the fluid yielded too much.

Significantly, the findings proved the hypothesis that implicit regularisation overcomes the inaccuracies associated with the explicit Papanastasiou regularisation for Bingham fluids. The success of the IR model helped confirm its applicability as an accurate and viable method for the direct numerical simulation of dense viscoplastic particle suspensions.

Contents

List of Figures

List of Tables

Chapter 1

Introduction

Due to their non-Newtonian rheological properties, viscoplastic fluid-particle suspensions are useful to industrial applications from hydraulic fracturing to pipeline particle transportation. Current semi-empirical and numerical techniques for the modelling and prediction of these suspensions' flows are, however, inaccurate and limited in their application, mainly due to the complex phenomena present in the interactions between particles and yield-stress fluids. Hence, this thesis project will assess the ability of an implicitly regularised model to numerically characterise the rheology of these suspensions, with a view to significantly improve the prediction of their behaviour in industrial applications.

1.1 Viscoplastic Fluid-Particle Suspensions

Compared to Newtonian fluids, the presence of a yield-stress in viscopastic fluids introduces numerous complexities to their interaction with solid objects. For example, with a high enough yield-stress, a particle's weight can be completely supported in a suspension, and rendered stationary relative to the fluid [1]. Existing numerical methods encounter significant difficulties when attempting to model the yield-stress problem, while the problem of continually updating particle boundaries presents a limitation to classical CFD methods. Hence, there are currently no comprehensive modelling strategies to characterise the rheology of dense fluid-particle suspensions. It is the desire to model the constitutive behaviour of these suspensions as a whole via direct numerical simulation (DNS) which provides the motivation for this project.

The investigation will apply coupled fluid-particle mechanics to achieve this, which itself utilises the lattice-Boltzmann method (LBM) and discrete element method (DEM) to model the fluid and particle components respectively. To solve the yield-stress problem, an implicit regularisation method is proposed, which is hypothesised to have significant performance benefits compared to current explicit regularisation methods. Hence, the validation and performance evaluation of the application of the implictly-regularised LBM-

DEM model to viscoplastic fluid-particle coupling is required.

1.2 Industrial Context

In recent years, the extraction of natural gas from coal seams and shale has emerged as a powerful, unconventional method of hydrocarbon production. With the benefits of a lower carbon footprint relative to other fossil fuels and its availability in abundance, natural gas is viewed as the bridge to a low-carbon future [2], substantiating the need for improved modelling of these unconventional processes.

The extraction of natural gases from coal seams and shale is facilitated by the creation, and propping open, of hydraulic fractures. Initially, after the creation of blast-induced paths within the fracturing medium, "a viscous fluid is pumped inside the wellbore, inducing a steep rise in the pressure which eventually leads to the initiation of a fracture at the perforated interval [3]." The propping process is then achieved through the transportation of "proppant" particles densely suspended within the injecting fluid which, when removed, causes the fracture to close in on the proppants.

Viscoplastic fluids can constitute the fluid component of the suspensions. The ability of these fluids to support the weight of particles, as described above, renders them particularly useful for transporting proppant from the wellbore to the fracture tip, while their lack of deformation below a certain shear stress facilitates the opening of fractures to the desired width for particle entrance [4]. This characteristic has also been utilised in the design of long distance slurry pipelines, where coarse solids have be transported in dense, viscoplastic fluids [5].

It is the importance of viscoplastic fluid-particle suspensions to these applications which provides the motivation for this project to model and predict these suspensions' behaviours.

1.3 Aims & Objectives

The aim of this thesis investigation is:

To asses and compare the performance of an implicitly-regularised model for the potential modelling of viscoplastic particle suspensions to current explicitly-regularised models.

In order to achieve this aim, the following objectives will be met:

1. Develop an understanding of the state-of-the-art theory behind and methods for the numerical characterisation of viscoplastic fluid-particle suspensions.

2. Design a campaign of models for the validation and performance evaluation of the implicitly- and explicitly-regularised LBM-DEM models.

1.4 Scope

Regarding the fluid input parameters, the yield-stress, viscosity and density were considered to be within the scope of the investigation. Additionally, Bingham fluids were the only suspension base-fluid considered, while spheres were the only particles considered. The investigation limited itself to the validation and performance evaluation of two LBM-DEM models, namely the implicit and Papanastasiou regularisations, while a maximum of two particles were considered.

In order to ensure that meaningful outcomes were achieved within the available time frame and resources of the thesis, the following parameters were considered to be out of the project's scope: the effects of temperature on the fluid's rheology as an input parameter; fluids which fell outside the Bingham model (e.g., Herschel-Bulkley fluids); irregular and non-spherical particles; and modelling of more than two particles (i.e., dense suspension rheology characterisation.

1.5 Chapter Summary

The second chapter gives a detailed analysis of the state-of-the-art literature pertaining to the viscoplastic fluid-particle coupling problem. Existing literature studies are critically evaluated as a means for validation and performance evaluation of the current models.

The third chapter outlines the methodology utilised to validate the current IR model and compare its performance to the PR TRT model. The results of these analyses are presented in chapter four, along with in depth evaluations of the numerical stability and parameter dependencies of each model.

The fifth chapter comprises a detailed discussion of the numerical findings, making the significance of these to the current work clear.

Finally, the investigation is summarised in chapter six, where the major findings are juxtaposed to clearly and concisely clarify the outcomes of the project and their significance to future work.

Chapter 2

Literature Review

2.1 Viscoplastic Fluid-Particle Interactions

This section describes the phenomena observed in particle interactions with viscoplastic fluids, with a view to validate the accurate capturing of these properties in the LBM-DEM model. Existing data from experimental and numerical studies was collated and critically analysed for use in the validation programme.

2.1.1 Yield-Stress Fluids

Newtonian fluids are fully characterised by a coefficient of viscosity, μ, which remains constant as the shear stress, τ, imparted on the fluid increases linearly with increasing strain rate, $\dot{\gamma}$,

$$\tau = \mu\dot{\gamma}. \tag{2.1}$$

Viscoplastic fluids are a type of non-Newtonian fluid which exhibit a yield-stress (i.e., resist a finite amount of stress before beginning to flow). The most basic model of a viscoplastic fluid is the Bingham fluid [6]. The yield-stress below which the fluid does not deform is introduced as τ_y, such that $\dot{\gamma} = 0$ for $\tau < \tau_y$, while the coefficient of viscosity is redefined as the plastic shear viscosity, μ_p (also a scalar constant), so that the fluid's shear stress above τ_y at a particular strain rate is given by,

$$\tau = \tau_y + \mu_p\dot{\gamma}. \tag{2.2}$$

The fact that no deformation occurs for any $\tau < \tau_y$, however, leads to the explicit solution of stress distributions in un-yielded regions becoming statically indeterminate [7]. The simplest way of overcoming this issue is the bi-viscosity model. As depicted in Figure 2.1,

the un-yielded region is re-modelled by a steep linear increase in τ up to a defined critical strain rate, $\dot{\gamma}_c$,

$$\tau = \mu_0 \dot{\gamma}, \tag{2.3}$$

where μ_0 represents the viscosity within this region [8]. For $\dot{\gamma} > \dot{\gamma}_c$, the fluid is then defined by the model described by Equation 2.2.

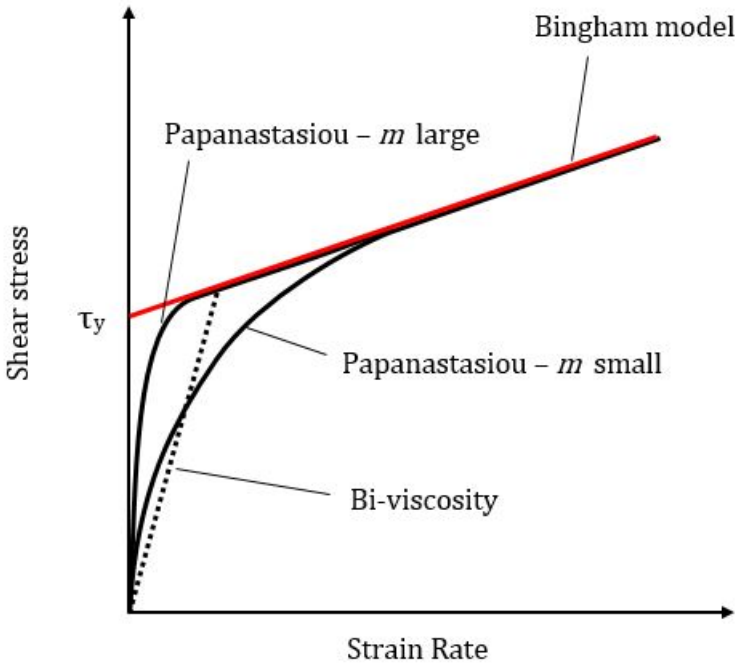

Figure 2.1: Illustration of the bi-viscosity and Papanastasiou regularisations compared to the constitutive Bingham model.

Another common approach for overcoming the discontinuos yield-stress problem is the Papanastasiou regularisation [9], which introduces a parameter, m (also referred to as the stress growth exponent), such that,

$$\tau = \tau_y(1 - e^{-m\dot{\gamma}}) + \mu_p \dot{\gamma}. \tag{2.4}$$

By inspection of Equation 2.4, the un-yielded, or zero-strain, region is eliminated, while the effective viscosity increases exponentially without reaching infinity as the strain rate approaches zero, allowing the new fluid model to be numerically implemented without the need for complex numerical techniques within traditional finite element methods. However, in all studies which take this regularisation approach, the stress growth exponent has been decreased significantly as the fluid's yield stress increases in order to ensure numerical stability [10–12]. Additionally, due to the elimination of a zero-strain region,

regions of un-yielded fluid are represented by creeping rather than completely stagnant flow. As a consequence of these approximations, the likeness of the regularised model to the true viscoplastic model is reduced, which can lead to inappropriate results.

For the LBM, which shall be discussed in further detail later in the review, there exists an additional regularisation method, whereby the fluid collision operators are specially constructed such that the stress and the shear rate satisfy Equation 2.2 simultaneously (i.e., the zero-strain condition is satisfied) [7]. This so-called "implicit" regularisation has been shown to be superior to the Papanastasiou regularisation in the application of the LBM model to Bingham fluid flows [13].

An additional class of viscoplastic fluids is characterised by the Herschel-Bulkley model,

$$\tau = \tau_y + \kappa\dot{\gamma}^n. \tag{2.5}$$

Unlike the Bingham model, shear stress is not linearly proportional to strain rate, and is instead dependent upon the power law index, n. The consistency, κ, represents the fact that viscosity varies as a function of $\dot{\gamma}$. The models described in Equations 2.2 and 2.5 are equivalent when $n = 1$.

2.1.2 Dimensionless Numbers

The two main dimensionless numbers used when analysing objects in Bingham fluids are the Reynolds number (Re) and the Bingham number (Bi),

$$Re = \frac{\rho_f U_c L_c}{\mu_p}, \tag{2.6}$$

$$Bi = \frac{\tau_0 L_c}{\mu_p U_c}, \tag{2.7}$$

where ρ_f, μ_p and τ_0 are the Bingham fluid density, plastic viscosity and yield-stress, respectively. The characteristic length of the object, L_c, is equal to the diameter, d, for spheres and cylinders, while U_c denotes the characteristic velocity of the flow configuration.

The drag coefficient, C_D, defined by Equation 2.9, was also utilised for a number of the validation models.

$$C_D = \frac{2F_d}{\rho_f U_c^2 A}. \tag{2.8}$$

Here, F_d denotes the drag force acting on the object, while A is the object's reference area which, for a sphere, is equal to its cross-sectional area.

For creeping flow it is more pertinent to utilise the Stokes' drag coefficient,

$$C_S = \frac{F_d}{6\pi\mu_p U_c r}, \tag{2.9}$$

when analysing drag force on a sphere, where r is equal to the sphere radius.

2.1.3 Two-Dimensional Fluid-Particle Interaction

As a precursor to validating spherical particle coupling to a Bingham fluid, flow in two dimensions can first be validated. When analysing 2-D flow, the cross section of an infinitely long cylinder and the corresponding 2-D flow properties becomes analogous to flow past a sphere in three dimensions.

2.1.3.1 Single Cylinder

The characteristics of Newtonian fluids have been studied extensively in the literature. Perhaps the most elementary study of fluid-particle interaction is that of a Newtonian flow past an infinitely long cylinder in two dimensions. Figure 2.2 depicts the results of a benchmark experimental study in which the drag on a infinitely long cylinder was measured for Re in the inertial flow regime. Specifically, an inverse linear relationship exists between the drag and Reynolds number low Re. At higher Re, however, the trend flattens, with the decrease in drag as Re is increased approaching zero. This data enables validation of the momentum characteristics of the current LBM-DEM model in the inertial regime.

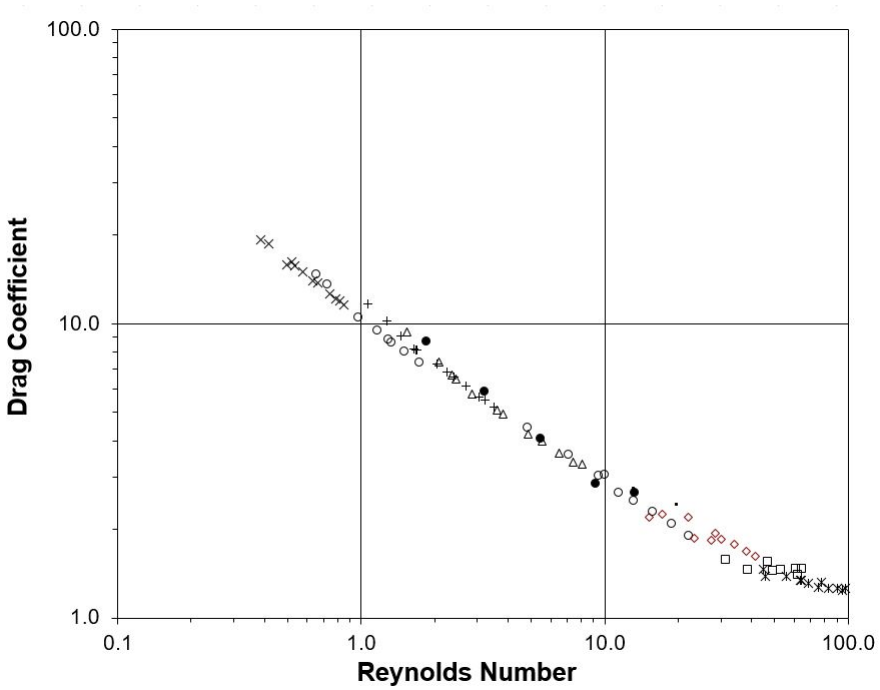

Figure 2.2: Drag coefficient of a cylinder over a range of 2-D, inertial Newtonian flows [14].

When moving from flows of Newtonian fluids to Bingham fluids, however, experimental and numerical studies become scarce. For 2-D Bingham flow past a cylinder in particular, only a handful of results exist. Table 2.1 displays the drag results obtained by a Papanastasiou-regularised finite element method at low Re and low to moderate Bi [15]. Like the Newtonian results presented above, a clear decrease in drag was observed with increasing Re. Notably, C_D was highly dependant upon the Bingham number, increasing as Bi was increased. These quantitative results closely matched the other known numerical study of Bingham flow past a single cylinder.

Table 2.1: Drag results, obtained by a Papanastasiou-regularised finite element method, for the flow of a Bingham fluid past a 2-D cylinder for low Re and Bi [15].

Re	$Bi = 1$	$Bi = 5$	$Bi = 10$
0.1	598.21	1950.1	3308.8
10	6.8994	19.405	33.105
20	3.9749	10.192	16.996
40	2.4262	5.5597	8.9614

2.1.3.2 Periodic Cylinder Array

While the above results have the potential to validate Bingham fluid-particle interaction, inter-particle hydrodynamic effects are still lacking. One modelling approach for the simulation of particle interactions is flow through a periodic array of stationary objects.

In a study investigating the creeping flow of a Bingham fluid past an infinite, orthogonal array of cylinders, the drag coefficient of the cylinders was correlated to the Bingham number of the fluid by solving the creeping flow equations using finite differences and the bi-viscosity approximation of the Bingham constitutive equation [16]. Drag results on a single cylinder as a base case were highly agreeable with results from a number of other studies.

The drag coefficient of a cylinder within the array, C_D, was calculated for simulations of varying solid area fraction, ϕ, and Bi. Figure 2.3 depicts the resulting C_D, from which the drag coefficient for the Newtonian case has been subtracted, plotted against increasing Bi.

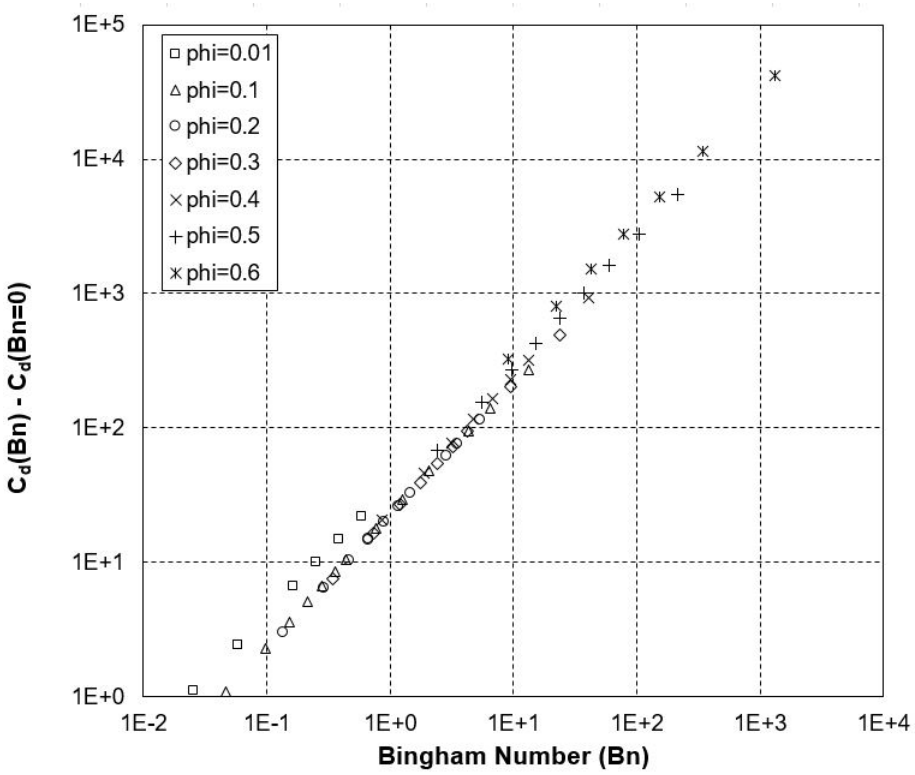

Figure 2.3: Cylinder C_D within an infinite, in-line cylindrical array, normalised against Newtonian case over a range of Bi [16].

Notably, an approximately linear relationship between normalised drag and Bingham number on the log-log scale can be observed, while the array of comparatively low solid area fraction, $\phi = 0.01$, exhibits markedly higher drag.

2.1.4 Three Dimensional Single Particle Flow Field

The next logical step for the validation of fluid-particle coupling in yield-stress fluids is to extend the 2-D array scenario to a 3-D situation; qualitative validation of the flow field around a single spherical particle represents the most elementary 3-D unit problem.

While no analytical solutions exist for the flow of a Bingham fluid past a stationary sphere, visualisation of the flow field has been documented by many numerical studies. Utilising a finite-element/Newton method, accurate predictions for the shapes of yielded and unyielded fluid flowing past a sphere in a cylindrical tube were first postulated. Particularly, it was noticed that, as Bi was increased, small solid caps at the poles of the sphere formed and grew [10].

In a subsequent numerical study utilising the Papanastasiou regularisation, this work was confirmed and extended by varying the ratio of the sphere diameter to that of the cylindrical tube (L/d) from 2:1 to 50:1, whilst again varying Bi at a constant Re [11]. Holding the sphere stationary, the test cell walls and fluid were moved at a constant velocity. The results for an 8:1 diameter ratio are presented in Figure 2.4.

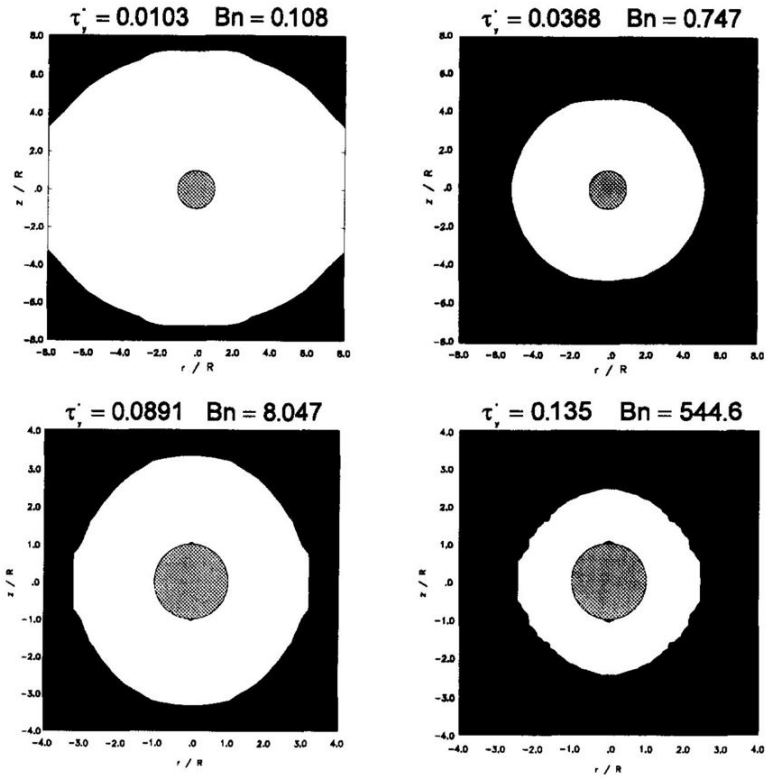

Figure 2.4: Variation of unyielded fluid zone (black) with increasing Bi for circular tube with 8:1 diameter ratio (flow from bottom to top of page) [11].

A number of other studies have reported similar results. Figure 2.5 illustrates flow fields obtained via two different LBMs [17, 18] for $Re = 0.001$ over a range of Bi. Each study utilised square-based-cylinder test cells of dimensions $4 \times 4 \times 6$ ($L/d \times L/d \times H/d$), where both the fluid and cell walls moved at a constant velocity past the stationary sphere. Notably, the multiple-relaxation-time model (MRT, to be discussed in more detail in Section 2.2.1) with Papanastasiou regularisation (b) predicted the formation of un-yielded regions to either side of the sphere and solid caps at the poles of the sphere at lower Bi than the bi-viscosity model (a).

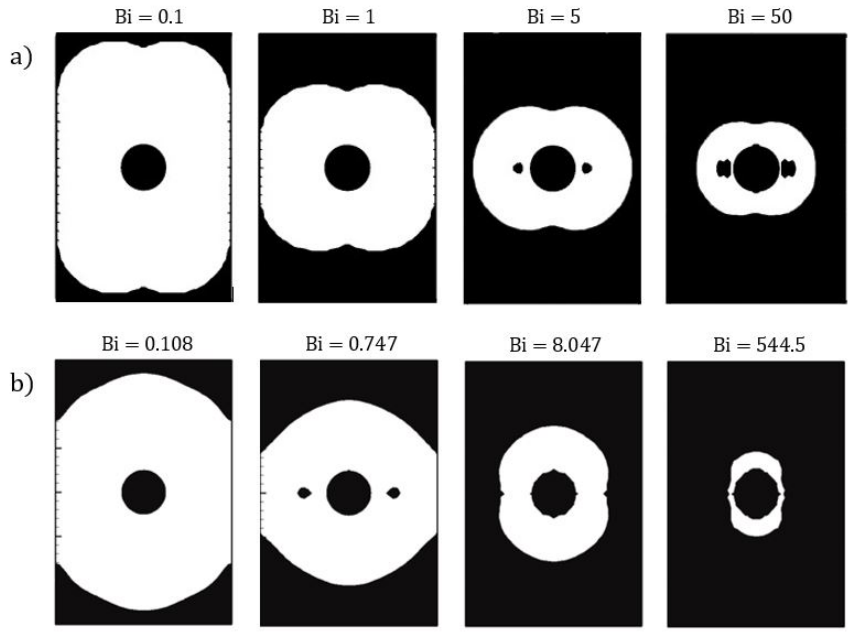

Figure 2.5: Variation of unyielded fluid zone (black) with increasing Bi for two LBMs utilising a) the bi-viscosity Bingham model [17] and b) a MRT method with Papanastasiou regularisation [18].

2.1.5 Particle Drag

The literature studies of drag on spheres can be sorted into two distinct categories: those in which fluid is forced at a constant rate past a fixed sphere; and those in which the solid particle is let to settle in a stationary fluid within a closed domain. The former method is nearly exclusively observed in numerical studies, while the majority of experimental drag coefficient studies concern themselves with a settling sphere.

2.1.5.1 Fixed Sphere

The creeping flow of a Bingham fluid past a fixed sphere has been investigated by many numerical studies, as presented in the previous section, all of which have simulated a domain with moving walls and fluid. Extending the qualitative results above, the drag effects of the yield-stress have also been quantified. Table 2.2 lists the Stokes' drag coefficient for creeping flow obtained by two prominent literature studies [10, 12] over a range of Bi. It should be noted that each of these studies utilised the finite element method, and as such employed the Papanastasiou regularisation to solve the yield-stress problem. The regularisation parameters, m, utilised by the latter study are also included.

Table 2.2: C_S values obtained over a range of Bi by two numerical studies using the finite element method and Papanastasiou regularisation [10, 12].

Bi	Beris et al.(1985)	Liu et al.(2002)	m
0.007	1.17	1.16	28490
0.108	1.74	1.74	19157
0.747	3.46	3.45	9634
2.299	6.39	6.38	5216
8.047	15.24	15.21	2190
14.91	24.85	24.85	13414
27.36	41.45	41.46	8042
59.59	82.77	82.67	4030
197.5	253.2	252.6	1316
340.7	426.9	426.0	781
544.6	669.7	671.9	496

Notably, the regularisation parameter becomes increasingly small as Bi is increased, in order to prevent numerical instabilities. This increasing approximation at high yield-stresses must inevitably introduce error into the results.

It must be noted that $Re = 0.1$ is the generally accepted upper limit for the creeping flow regime of a Bingham fluid [1].

2.1.5.2 Settling Sphere

Many experimental studies have investigated the drag force acting on a settling sphere in a stationary Bingham fluid within a slip tube. A primary concern of these early experimental studies was the development of an empirical formula relating the non-dimensional drag coefficient of a sphere to the Bingham fluid yield-stress. After the notion that C_D was dependant upon the yield-stress and dynamic forces of the fluid acting on the particle, the modified Reynolds number, Re^*, was developed [19] in order to quantify inertial, viscous and yield-stress forces concurrently,

$$Re^* = \frac{Re}{1 + Bi}. \tag{2.10}$$

Figure 2.6 depicts the terminal drag coefficient results from a number of the prominent experimental studies, ranging from creeping to inertial flow, plotted against Re^*. Also included are the results of a recent numerical study, which utilised the finite element

method with the Papanastasiou regularisation [20].

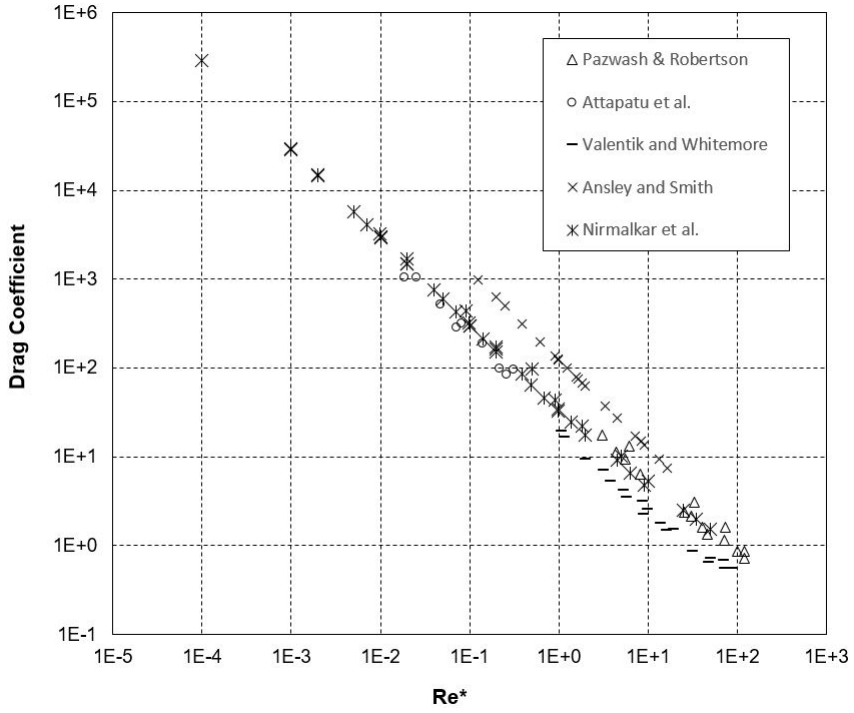

Figure 2.6: C_D for a sphere settling in a slip tube over a range of inertial and yield-stress conditions from prominent literature and experimental studies [20–24].

Based on the modified Reynolds number presented above, an experimental drag correlation for Bingham fluids, perhaps the most successful to date [22], was developed [21],

$$C_D = \frac{34(1 + \frac{7\pi}{24}Bi)}{Re}. \tag{2.11}$$

However, equation 2.11 is only accurate for $Re^* < 20$, after which the results deviate significantly. In the numerical study mentioned above, an additional drag correlation pertinent to the inertial regime was proposed [20],

$$C_D = \frac{28.63}{Re^*}(1 + 0.19Re^{*0.33}). \tag{2.12}$$

It must be noted that for any study of flow past an object within a finite domain, be it experimental or numerical, there will exist some wall effects due to the finite domain size, however large. Hence, discrepancies between experimental investigations can somewhat be explained by wall effects; it is pertinent to quantify and, if possible, eliminate the error they introduce. As an example, in later experimental studies of a settling sphere in a Herschel-Bulkley fluid [22, 25], it was observed that for a rectangular test cell of square cross section, a cell width to sphere diameter ratio of 10 was sufficient to negate wall effects. This is supported by numerical flow field visualisations for Bingham fluids [11].

For an object falling at terminal velocity through a fluid, buoyant and drag forces balance the force due to gravity. Hence, after experimentally measuring the terminal velocity U_T of a falling sphere, its drag coefficient can be determined as,

$$C_D = \frac{4gd(\rho - \rho_f)}{3\rho_f U_T^2}, \tag{2.13}$$

where ρ and ρ_f are the particle and fluid densities respectively.

An additional aspect of the settling sphere problem with which numerical and experimental studies have concerned themselves is the yielding limit. Due to the yield-stress of a Bingham fluid, a particle will not exhibit motion until the gravitational force has overcome the resisting yield force. While the ratio of gravitational-to-yield forces has been quantified in numerous ways, the simplest is given as [1],

$$Y_G = \frac{\tau_0}{gd(\rho - \rho_f)}. \tag{2.14}$$

Hence, the critical value for which a sphere will remain stationary when released in a Bingham fluid is introduce as $Y_{G,crit}$. Some experimentally and numerically observed values of $Y_{G,crit}$ are presented in Table 2.3. It should be noted that each of the numerical studies used some form of explicit regularisation, and were unable to directly observe the non-yielding phenomena; the yielding point was calculated by means of solving the relationship between C_S and Y_G for the critical yielding parameter as drag tended to infinity.

Table 2.3: Reported literature values of the gravity-to-yield parameter, $Y_{G,crit}$ [1].

Author	Study Type	$Y_{G,crit}$
Ansley & Smith (1967)	Experimental; settling sphere	0.068 - 0.084
Beris et al. (1985)	Finite Element Method	0.048
Atapattu et al. (1986)	Experimental; settling sphere	0.095 - 0.111
Blackery & Mitsoulis (1997)	Finite Element Method	0.048
Merkak et al. (2006)	Experimental; sphere pulled at constant velocity	0.062 - 0.088
Chen et al. (2016)	Lattice Boltzmann Method	0.046

2.1.6 Interaction Between Two Identical Spheres

A number of numerical studies have been conducted investigating the hydrodynamic interaction between two spheres in Bingham fluids, formulating the problem with both fixed [26] and settling [17, 27] spheres. The settling sphere studies , however, calculated Bi and Re based off the characteristic Stokes velocity of the settling particle, such that the terminal Bingham and Reynolds numbers varied between tests with the terminal settling velocity. As such, they obtained qualitatively opposing results to that of the constant Re and Bi fixed sphere study. Hence, for the fixed sphere implementation of this investigation, the fixed sphere literature study shall be utilised for validation.

Utilising an explicitly regularised finite element method, two spheres of radius R were fixed at a distance L apart in a creeping Bingham fluid flow. The average drag acting on the spheres was then measured, from which C_S was calculated. At a constant $Bi = 340.7$, C_S was calculated for a number of sphere separating distances, which were normalised by the single sphere drag solution, $C_{S,single}$. The results are presented in Figure 2.7. Clearly, the sphere interaction effects were much less for the Bingham fluid compared to the Newtonian fluid case, with no interaction occurring for $L/R \geq 6$.

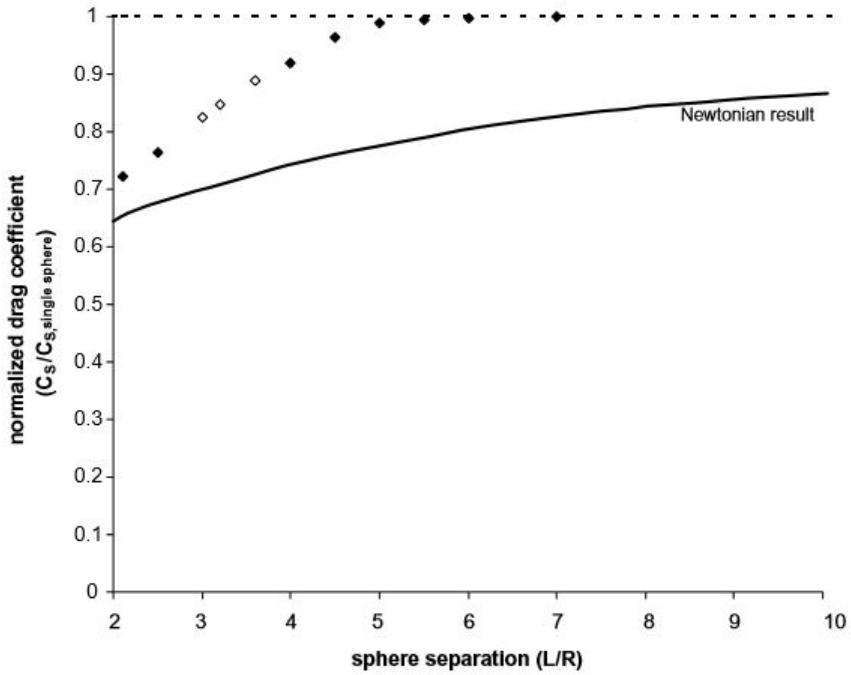

Figure 2.7: Normalized drag coefficients ($C_S/C_{S,single}$) for two spheres interacting co-linearly in a creeping Bingham flow of $Bi = 340.7$ for increasing separation distance [26].

In addition to these quantitative results, visualisations of the yielded and un-yielded regions surrounding the spheres were reported (Figure 2.8). For small L/R, an un-yielded region connecting the spheres is evident. As the separating distance is increased, this region diminishes, eventually detaching from the spheres but remaining as a sort of plug.

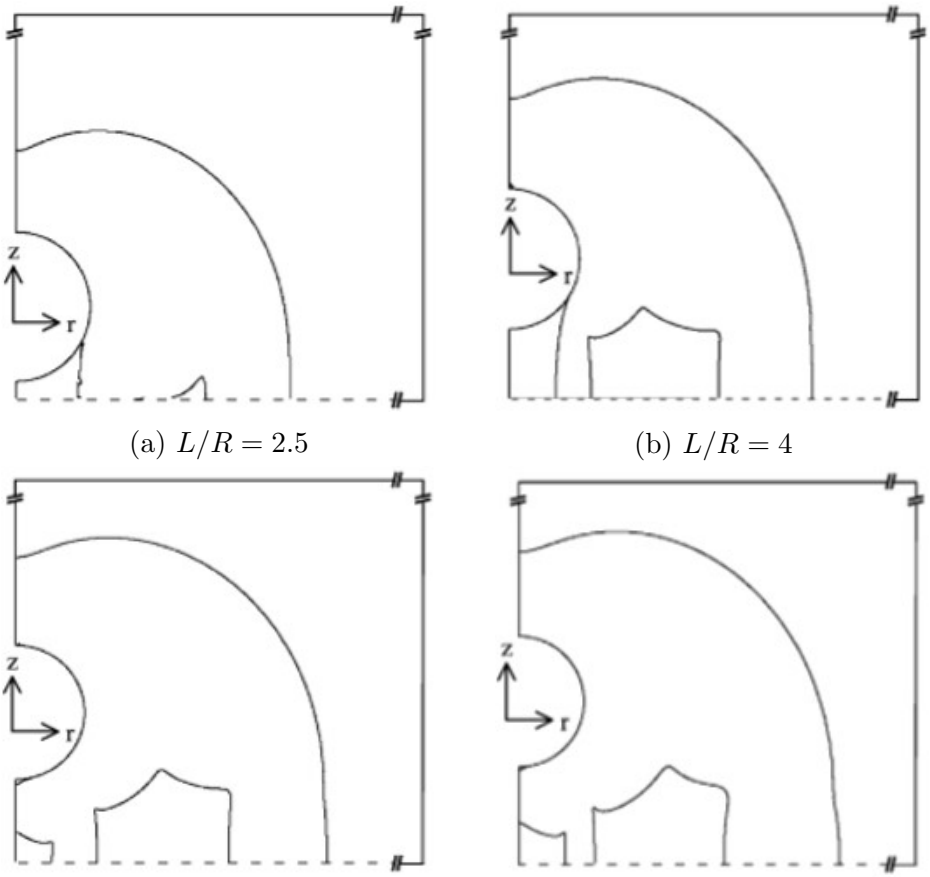

(a) $L/R = 2.5$ (b) $L/R = 4$

(c) $L/R = 4.5$ (d) $L/R = 5$

Figure 2.8: Variation of un-yielded region connecting two co-linear spheres in a creeping Bingham flow at $Bi = 340.7$ [12].

2.1.7 Rheology of Dense Suspensions

When particles are added to any fluid to create a non-colloidal suspension, numerous complexities arise when attempting to achieve explicit numerical modelling, especially in the dense regime. In Newtonian fluid-particle suspensions alone, phenomena such as fluid-solid interactions, like drag and fluid deformation, and solid-solid collisions are difficult to capture with accuracy. Currently, the direct numerical simulation of these suspensions has been successful utilising coupled fluid-particle mechanics [28]. This method shall be presented in further depth later in the literature review.

When the study of these suspensions is extended to non-Newtonian yield-stress fluids, however, the complexity further increases due to the presence of a yield-stress. As discussed above, the presence of a yield-stress significantly affects the drag forces on particles. Similarly, the flow field generated by a moving particle is significantly different to that in a Newtonian fluid [1].

These complications manifest in the overall characteristics of viscoplastic particle suspensions when the solid volume fraction (ϕ) approaches the packing limit. In this situation,

numerous experimental studies have documented that the overall suspension yield stress changes significantly from that of the base fluid's, with explanations for this phenomena remaining speculative [29, 30]. Further studies concluded that "the properties of the viscoplastic suspensions can be satisfactorily modelled as those of a Herschel–Bulkley fluid with an exponent equal to that of the suspending fluid, with the dimensionless effective yield stress and consistency being sole functions of ϕ [31, 32]."

2.2 Numerics

After the identification of the difficulties of Bingham fluid-particle modelling in traditional computational fluid dynamics (CFD) methods above, the LBM-DEM shall be presented here as a potentially superior method for coupling particles to viscoplastic fluids. The LBM is implemented to model the yield-stress fluid phase of the suspensions, while the DEM is implemented in parallel with the LBM to simulate the suspensions as a whole. A description of the respective modelling methods, along with their application and suitability to the modelling task, is presented below.

2.2.1 Lattice-Boltzmann Method

When attempting to numerically model yield-stress fluids, numerous complexities arise due to discontinuity inherent with the presence of the yield-stress. As discussed, classical CFD approaches are inaccurate or cumbersome for large Bi or when attempting to model complex geometries and boundary conditions. The LBM, however, presents a highly attractive method for modelling Bingham fluids, due to the relative simplicity of its formulation and application and its high level of computational parallelisation [33].

Rather than discretising and solving the Navier-Stokes equations as with classical CFD methods, the LBM takes a kinetic approach to solving fluid movement, in which the modelled fluid is made up of lattice sites, each containing a set of specially chosen velocity vectors, c_i. The movement of fluid through the lattice sites is described by the propagation of particle distribution functions, f_i, along the c_i, such that the governing hydrodynamic properties (density, momentum and momentum flux) are recovered [13]. This is represented mathematically by the lattice Boltzmann equation (LBE), given in its discretized LBM form as,

$$f_i(t + \Delta t, \boldsymbol{x} + c_i \Delta t) - f_i(t, \boldsymbol{x}) = \Omega_i(\boldsymbol{f}), \tag{2.15}$$

where $\boldsymbol{x_j}$ are the lattice site position vectors and $\Omega_i(\boldsymbol{f})$ is the collision operator, which updates the distribution functions at the new lattice position. For these, "almost all lattice Boltzmann models use the relaxation time approximation" [34], where the particle distribution functions are relaxed towards their equilibrium values, f_i^{eq}.

The most simple and hence commonly used collision operator up to this point is the Bhatnagar-Gross-Krook (BGK) model,

$$\Omega_i(\boldsymbol{f}) = -\frac{1}{\tau}(f_i - f_i^{eq}), \tag{2.16}$$

which utilises a single relaxation rate, τ. An additional type of collision operator is the multiple relaxation time (MRT) method, so named due to its application of a unique relaxation rate to each distribution function. Specifically, f_i and f_i^{eq} are transformed into hydrodynamic moments by the moment matrix, $\mathbf{M}$, while all relaxation rates are contained within the diagonal matrix, $\mathbf{S}$ [35], so that the collision operator is represented as,

$$\Omega_i(\boldsymbol{f}) = -\sum_{j=0}^{N-1}(\boldsymbol{M^{-1}SM})_{ij}(f_j - f_j^{eq}). \tag{2.17}$$

Compared to the BGK method, this use of multiple relaxation parameters can afford modelling of new parameters such as the Prandtl number, improved stability and accuracy, and greater control over boundary conditions; depending on the modelled problem at hand and the selected parameters, however, "MRT can be both more accurate and stable than a single relaxation time (BGK) LBE or less so" [34]. Pertaining to the problem of viscoplastic fluids, the use of two specially chosen relaxation times, commonly referred as the TRT model, has been shown to eliminate the spurious boundary and non-hydrodynamic effects present in the BGK formulation, while maintaining the same computational efficiency and simplicity [36].

As previously mentioned, there exists an additional, implicit, regularisation model (IR) for the LBM, separate to the explicit BGK and TRT collision operators presented above, in which particle distribution functions and the fluid's yield-stress are simultaneously updated at the collision step. At this point, it must be made clear that the LBM actually utilises a transformed set of particle distribution functions,

$$\bar{f}_i(\boldsymbol{x}, t) = f_i(\boldsymbol{x}, t) - \frac{\Delta t}{2}\Omega_i(\boldsymbol{x}, t). \tag{2.18}$$

In the IR formulation, the f_i^{eq} are subtracted from Equation 2.18, of which the second moment is then taken. Ultimately, this relates the second moment of the collision operator and transformed particle distribution functions, $\boldsymbol{s}$ and $\boldsymbol{T}$, to the fluid stress, $\boldsymbol{\sigma}$,

$$\frac{\Delta t}{2}\boldsymbol{s} + \boldsymbol{T} = -\boldsymbol{\sigma}. \tag{2.19}$$

As $\boldsymbol{T}$ are known quantities, $\boldsymbol{s}$ and $\boldsymbol{\sigma}$ may then be calculated depending on whether each T is below or exceeds the fluid's yield-stress. Finally, the post-collision particle distributioin functions are determined.

For a full description of this scheme, refer to Regulski et al. (2016), where its superiority over the PR -BGK and -TRT models has been demonstrated for simplified Bingham fluid flow scenarios. This investigation aims to extend this validation and superiority demonstration of the IR-LBM to Bingham fluid-particle coupling in three dimensions, with a view to its application to modelling dense viscoplastic particle suspensions.

2.2.1.1 Lattice Stencils

In 2-D modelling cases, such as the cylindrical array validation experiment which will be presented below, a nine-velocity lattice stencil (depicted in Figure 2.9), commonly referred to as the D2Q9 model, is almost always used [13].

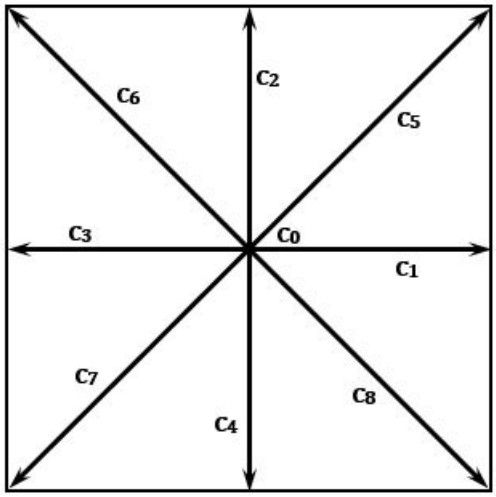

Figure 2.9: D2Q9 LBM lattice velocity set.

For the 3-D scenario, the most commonly used lattice models are the D3Q15 and D3Q19. While stencils with a lower number of velocities result in greater computational efficiency, numerous recent studies have documented non-axisymmetric solutions when the 15 or 19 velocity models are used to model the axisymmetric flow of yield-stress fluids at moderate to high Re [34]. When the D3Q27 model has been applied, however, these spurious effects are mostly eliminated. As a result, the D3Q27 stencil (as pictured in Figure 2.10) has emerged as an increasingly popular formulation in recent studies for the 3-D LBM modelling of viscoplastic fluids.

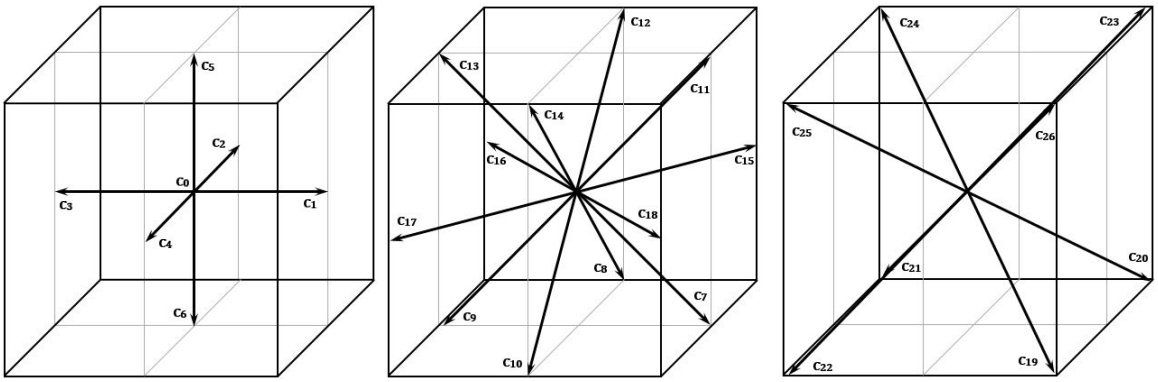

(a) (b) (c)

Figure 2.10: D3Q27 LBM lattice velocity set.

2.2.2 Discrete Element Method

The DEM aims to accurately model the movement of and interaction between macroscopic particles by stepping through the solving of constitutive equations and iteratively updating their positions.

The external forces which govern the motion of particles can be viewed as comprising hydrodynamic, electrostatic and gravitational forces. In order to cope with particle interaction, a simplified overlapping approach can be taken, whereby particle boundaries are assumed to remain un-deformed and the interaction forces are calculated as elastically proportional to the overlapping of the particle boundaries. Ultimately, the above forces can be implemented into Newton's equations of translational and rotational motion, as per Equations 2.20 and 2.21, to completely describe the movement of each particle, j [37],

$$m_j \boldsymbol{a_j} = \sum \boldsymbol{F_j}, \tag{2.20}$$

$$I_j \boldsymbol{\alpha_j} = \sum \boldsymbol{T_j}. \tag{2.21}$$

Tracking particle motion is then a matter of integrating these equations to solve for particle position through time. This scheme generally consists of four main steps [38, 39]. Firstly, a search is undertaken in order to determine which particles are likely to be in contact with other particles or boundaries. Secondly, the particle geometries and positions are utilised to calculate any overlaps between the previously identified particles, from which interaction forces are determined. Next, all external forces acting on each particle i, including interaction forces just calculated, are summed, providing the force and torque vectors, $\boldsymbol{F_i}$ and $\boldsymbol{T_i}$. Finally, Equations 2.20 and 2.21 are numerically integrated to attain the position of each particle at the current time step.

Numerical integration methods typically apply a forward-in-time, centred-in-space (FTCS) method in order to achieve solution stability, also utilising half time velocities to ultimately

calculate the updated particle position at the next time step.

Hence, with the capability to model and track the movement of multiple particles through time over a spatial domain, the DEM provides an excellent modelling strategy for the particulate component to yield-stress suspensions. Its parallel implementation with the LBM to achieve this is presented next.

2.2.3 LBM-DEM Coupling

The LBM can be efficiently and robustly coupled to a large number of discrete elements in comparison to classic CFD methods [40]. This is largely due to similarities between the LBM and DEM, in which the movement of fluid and particles is solved by iteratively updating their positions. Fluid-solid interactions can be grouped into two categories: stationary boundaries, such as fixed boundaries and stationary particles; and moving boundaries, which are present with non-stationary particles. Presented here are two of the main methods used for LBM-DEM coupling in these scenarios.

Pertaining to the problem of fixed solid boundaries, "in a typical LBM model, the bounce-back (BB) boundary condition is widely used to enforce the no-slip condition at the boundary interface" [28]. The key strength of this method is its numerical simplicity in modelling geometrically complex fluid-solid interfaces. As the name implies, when a fluid particle distribution function reaches a node designated as a fluid-solid interface, it is sent back directly from the direction it came. There are two main variations of BB, known as the on-grid and mid-grid methods. The principal difference in their formulations is the placement of the solid nodes. Unlike the on-grid formulation, in which the boundary node lies directly on the boundary, the mid-node method positions the solid boundary mid-way between the fluid node and a fictitious solid node, to which the fluid is streamed. While the mid-grid BB is computationally more expensive compared to the on-grid method, it exhibits second order accuracy (compared to the first order of on-grid) due to its centred nature [41].

Not only does BB have difficulty updating continuously evolving moving boundaries, it also gives no consideration to the sub-grid fluid-solid lattice features, greatly reducing the accuracy of the solution [28]. In order to overcome these issues, the immersed moving boundary (IMB) formulation was proposed [42]. Introducing a fluid-solid fraction term, B_n, the proportion of each lattice site which is fluid and solid is calculated. An additional solid collision operator, Ω^S, is also introduced, for which multiple formulations exist. Overall, the modified governing LBE is expressed as,

$$f_i(t + \Delta t, \boldsymbol{x} + c_i \Delta t) = f_i(t, \boldsymbol{x}) - (1 - B_n)(f_i^+(t, \boldsymbol{x})) + B_n \Omega_i^S, \tag{2.22}$$

where f_i^+ are the post-collision particle distribution functions.

The hydrodynamic force acting on each particle, j, can then be calculated,

$$F_j = \frac{\Delta x^2}{\Delta t} \sum_n B_n (\sum_i \Omega_i^S \boldsymbol{c_i}). \tag{2.23}$$

Similarly, the hydrodynamic torque is also calculated,

$$T_j = \frac{\Delta x^2}{\Delta t} \sum_n (x_n - x_j) B_n (\sum_i \Omega_i^S \boldsymbol{c_i}), \tag{2.24}$$

where $(x_n - x_j)$ is the distance between the solid boundary nodes and the particle centre. These hydrodynamic F_j and T_j can then be incorporated into Equations 2.20 and 2.21 for the DEM calculation of particle movement.

Chapter 3

Methodology

Before the coupled fluid-particle mechanics code can be applied to suspension characterisation, it was imperative that the present LBM-DEM models accurately captured the phenomena present in viscoplastic fluid-particle interactions. For the complexities which arise with the presence of the yield-stress of Bingham fluids in particular, this required comprehensive analysis of a number of benchmark fluid-particle coupling scenarios. Hence, the validation programme was developed by assessing simplified unit problems of the overall suspensions, for which a vast range of experimental and numerical results exist, as presented in Chapter 2.

An additional key aspect of the validation investigation was to prove the hypothesis that the implicitly regularised LBM-DEM model is superior in modelling viscoplastic fluids compared to the Papanastasiou-regularised TRT model. Hence, the following validation simulations were all conducted using each of these regularisation methods.

To assess the robustness of the models, the simulations were conducted for flows in the creeping and low inertial regimes, where $0.01 < Re < 200$. This enabled investigation and validation of a wide range of momentum, viscous and yield stress hydrodynamic effects.

3.1 Two-Dimensional Fluid-Particle Interaction

As a precursor to viscoplastic fluid-particle coupling validation in three dimensions, simulations for the simplified 2-D case were first conducted. For each of the 2-D scenarios evaluated, the particles took the form of cylinders. In the first, the drag effects of Newtonian flow past an infinitely long single cylinder were investigated, the results of which were compared to existing experimental data. This was then extended to Bingham fluids. Finally, the drag force imparted by a Bingham fluid on a periodic array of cylinders was measured.

3.1.1 Single Cylinder

Before validating the research code's ability to couple a yield-stress fluid to a particle, the flow was restricted to a Newtonian fluid, in order to ensure that hydrodynamic effects were correctly modelled. As depicted in Figure 3.1, modelling a single cylinder, a test cell with slip walls and a pressure outlet was implemented. Fluid entered at a constant velocity, V, at the inlet, taken as the characteristic velocity, U_C, while the force acting on the particle was directly measured.

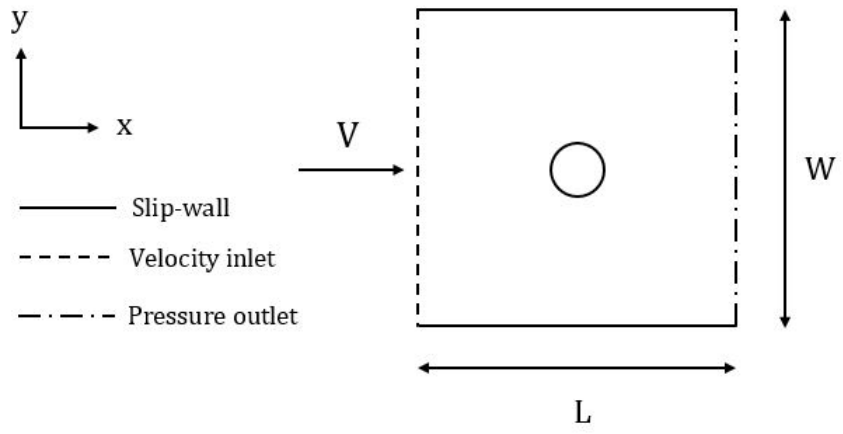

Figure 3.1: 2-D single cylinder test cell schematic.

In order to replicate the data of Tritton [14], τ_y was set to 0. At constant domain and cylinder dimesnions, the fluid was forced past the cylinder at increasing V to simulate a range of flows in the inertial regime (i.e., $0.3 < Re < 100$), for which the drag force acting on the cylinder was calculated.

Moving on to Bingham fluid flows, extending the flow from a Newtonian to a viscoplastic fluid ensured that yield-stress effects were validated. Again utilising the above test cell, the inlet fluid velocity and fluid yield-stress were varied to facilitate comparison to the literature data for low inertial Re and Bi. This was conducted utilising both the TRT Papanastasiou and implicit regularisations of the present LBM-DEM model, with a view to comparing their performance for the 2-D scenario.

Finally in the single cylinder simulation, the yield-stress effects on the vortex shedding characteristics of a Bingham fluid were investigated, for which no results currently exist in the literature.

3.1.2 Bingham Flow Through an Array of Cylinders

The next validation experiment investigated the flow of a Bingham fluid past an infinite orthogonal 2-D array of cylinders. Principally, the periodic array introduced inter-particle hydrodynamic interactions.

The infinite array was modelled utilising a square domain containing a single cylinder with periodic boundaries on all sides, as depicted in Figure 3.2. Fluid was forced through the test cell at a constant acceleration, g. The characteristic velocity, U_C, was calculated by averaging the integral velocity over the cell to the cell average velocity. To facilitate comparison to the study of Spelt et al. [16], the Reynolds number was defined with the periodic domain length, L, as the characteristic length, while the cylinder radius, rather than the diameter, was utilised as L_C in the calculation of Bi.

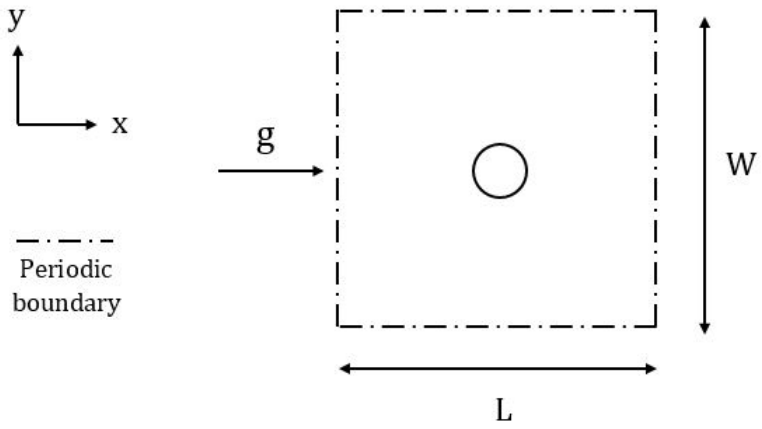

Figure 3.2: 2-D periodic cylinder array test cell schematic.

In order to replicate the data from Spelt et al. [16], the solid area fraction was varied between $\phi = 0.01, 0.1, 0.2, 0.3, 0.4, 0.5, 0.6$, by modifying the cylinder diameter at a constant, square, domain size. For each value of ϕ, the drag coefficient was calculated for the base Newtonian case (Bi=0). Bi was then varied between $0 < Bi < 1000$ by altering the fluid's yield-stress, from which the drag coefficient was calculated and the Newtonian drag subtracted.

In keeping with the literature study, the above procedure was conducted for $Re << 1$ to restrict the flow to the creeping regime; however, in order to validate the robustness of the LBM-DEM model, Re was also increased into the inertial regime. Eventually, the upper bounds on the stability as a consequence of increasing Re and Bi were investigated.

3.2 Three-Dimensional Fixed Sphere

Following the successful validation of yield-stress fluid-particle interactions in two dimensions, 3-D scenarios were considered.

3.2.1 Single Particle Flow Field

As a first qualitative assessment, the yielded and un-yielded regions of a creeping flow around a fixed sphere were compared to those in the literature [11, 17, 18].

As depicted in Figure 3.3, a stationary sphere was centred in a test cell with slip walls, a zero-gradient pressure outlet, and a constant velocity inlet. 30 cells were used for the sphere diameter, while the fluid's viscosity, ν, and velocity, V, were chosen such that $Re = 0.1$, representing the generally accepted upper limit for creeping flow. In order to replicate the moving walls simulated in the studies in the literature, relatively complex boundary modelling is required. Hence, with a view to simple numerical boundary implementation for the purpose of this investigation, the cell walls were modelled as stationary slip boundaries.

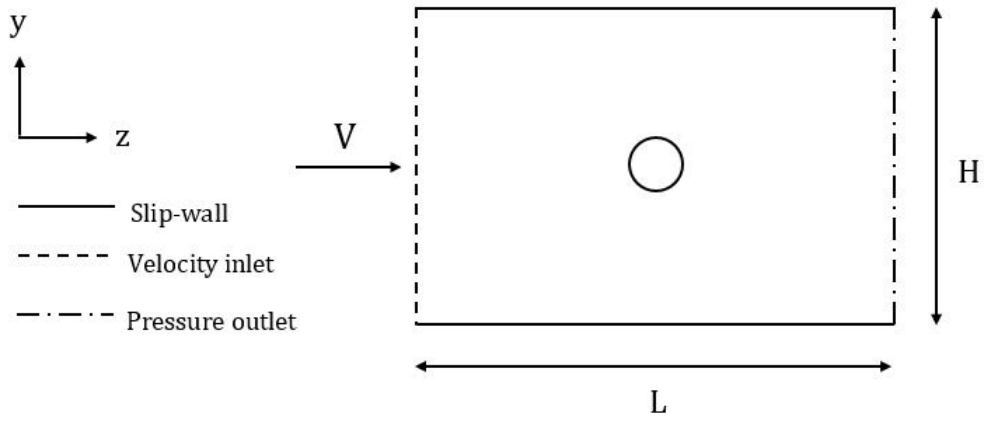

Figure 3.3: Single stationary sphere test cell section schematic.

Choosing to model the boundary conditions in this way, however, induced a non-linear velocity profile near the walls, causing the flow field to deviate significantly from those in Figure 2.5. Hence, in order to minimise these wall effect, a domain size of $10.6 \times 10.6 \times 6$ ($H/d \times H/d \times L/d$) was implemented.

Simulations were run for Bingham numbers of 0.1, 1, 5 and 10, which were set by varying the fluid yield-stress.

3.2.2 Creeping Drag Forces

Following the qualitative assessment of 3-D flow past a fixed sphere, the viscoplastic fluid-particle interactions were then quantitatively compared to literature data via the measurement of drag forces in the creeping flow regime.

The same test cell as depicted in Figure 3.3 was utilised. Before data was collated, a domain independence study was required to ensure that the test cell was sufficiently large such that the fixed walls did not interfere with the flow, and if they did, that any error associated with wall effects was quantified. This was conducted by initialising the domain with a sphere diameter, d, of 20 cells, and a domain size of $2d \times 2d \times 4d$ ($H \times H \times L$). The domain size was then increased to $3d \times 3d \times 6d$, $4d \times 4d \times 8d$, and so on, until the limit of computational memory was reached. This was conducted for $Bi = 1$ and $Bi = 100$ in order to quantify the effect of the yield-stress on wall interactions.

Following confirmation of domain independence, a grid sensitivity analysis was needed in order to observe the effect of grid resolution on the convergence of results. This was conducted at constant H/d again for $Bi = 1$ and $Bi = 100$.

Fluid was forced through the test cell at a velocity of 0.001 m/s in order to ensure that $Re << 1$. The fluid's yield-stress was then varied such that $0.007 \leq Bi \leq 544.6$ over a number of simulations, for each of which the drag force was measured and C_S computed, such that drag results from the literature were replicated [10, 12].

3.3 Single Settling Sphere

A number of experimental studies were identified in the literature for a sphere settling in a stationary Bingham fluid within a slip tube. Hence, in order to facilitate comparison with these, the next validation model implemented a fully enclosed cylindrical domain containing a stationary Bingham fluid, upon which a body force in the z direction, akin to gravity, was applied. As depicted in Figure 3.4, a sphere was initialised at the top of the domain and let to settle until it reached its terminal velocity.

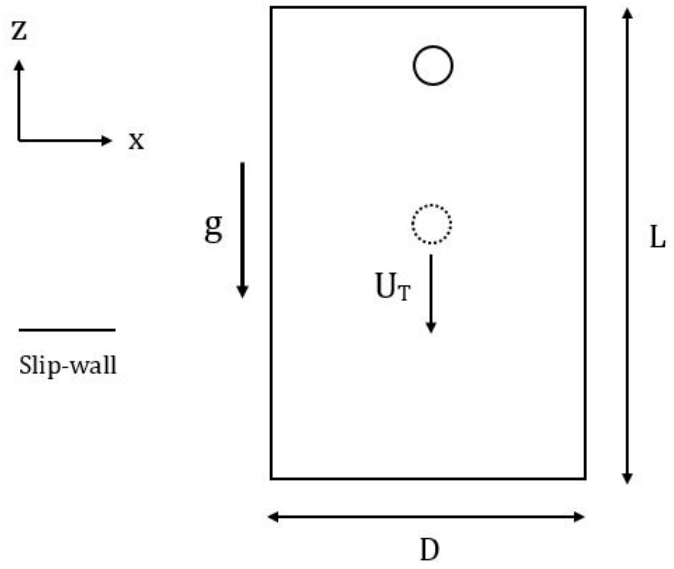

Figure 3.4: Single settling sphere test cell section schematic.

3.3.1 Yielding Limit

A common aspect of falling sphere studies in the literature is to investigate the yield-stress at which the gravitational force is countered by the equal and opposite yielding force, such that the sphere remains stationary. Hence, as part of this validation experiment, the fluid yield-stress was increased as all other parameters were held constant, until the particle exhibited no motion. From this critical yield stress value, $\tau_{y,crit}$, the gravitational-to-yield

force parameter, Y_G, was then calculated as per Equation 2.14, and compared to the values obtained in prominent studies.

3.3.2 Terminal Drag Forces

The next stage of the settling particle experiment observed the terminal drag force on a settling sphere in a Bingham fluid over a range of Re and Bi, facilitating comparison to existing benchmark studies in the inertial regime. In order to concurrently correlate the settling drag force to the inertial, viscous and yield-stress properties of the fluid, the non-dimensional modified Reynolds number, Re^* (Equation 2.10), was utilised, as per and facilitating comparison to the prominent experimental and numerical studies in the literature. The terminal settling velocity of the sphere, U_T, was taken as the characteristic velocity, U_C, from which Re and Bi were determined. C_D was calculated utilising the terminal buoancy expression presented in Equation 2.13. The terminal velocity was varied by increasing/decreasing the sphere density.

Before collating data, however, a grid sensitivity analysis was conducted for the settling sphere scenario in order to quantify the effect of grid resolution on the settling characteristics of the sphere. This was performed at a relatively low Re^*, ensuring that wall effects were not present in the analysis.

When handling the problem of wall effects, a trade-off between grid sensitivity and domain size-to-sphere diameter ratio was introduced due to the limited computational memory available. At high Re in particular, wall effects became more prominent, while the domain length required fore the sphere to reach terminal velocity without experiencing floor effects increased. Hence, it was pertinent to quantify their magnitude, allowing comparison to grid sensitivity effects and an informed decision of required domain size.

3.4 Interaction Between Two Identical Spheres

After ensuring that the IR LBM-DEM model correctly simulated viscoplastic fluid-particle interactions, the final validation experiment analysed hydrodynamic interactions between two particles. In order to achieve this, two fixed spheres were initialised in a domain identical to that of the single fixed sphere experiment, through which a Bingham fluid flowed at a constant velocity, V. As depicted in Figure 3.5, the spheres were positioned at a centre-to-centre distance, W, apart.

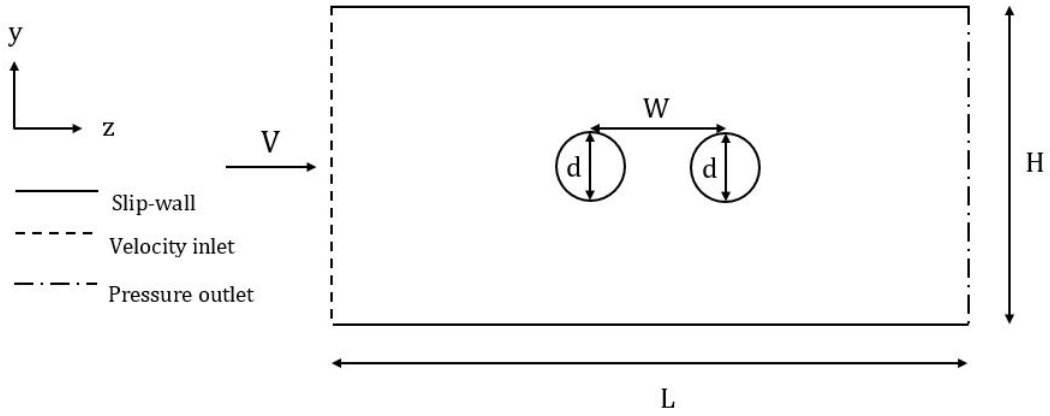

Figure 3.5: Sphere interaction test cell section schematic.

In order to investigate the interaction characteristics for Bingham fluids, flows for $Bi = 1, 10$ and 100 were simulated. As in the literature studies, the flow was restricted to the creeping regime. Consequently, the pertinent domain size and grid refinement determined for the single sphere scenario was also utilised here.

The sphere separation distance, represented as W/d, was systematically increased until no interaction effects were observed. The average Stokes drag coefficient of the spheres, C_S, was calculated for each W/d. After obtaining the drag solution for the single sphere scenario, the recorded drag results were normalised as $C_S/C_{S,single}$ to facilitate comparison to the literature results.

Chapter 4

Results

4.1 Two Dimensional Fluid-Particle Interactions

4.1.1 Single Cylinder

As the preliminary experiment for validation in two dimensions, the drag force imparted on an infinitely long cylinder by an inertial, Newtonian fluid flow was measured over a range of flow conditions. Figure 4.1 compares drag results over the range $0.3 < Re < 100$, obtained using the IR collison operator and IMB fluid-cylinder interface, to the study of Tritton [14].

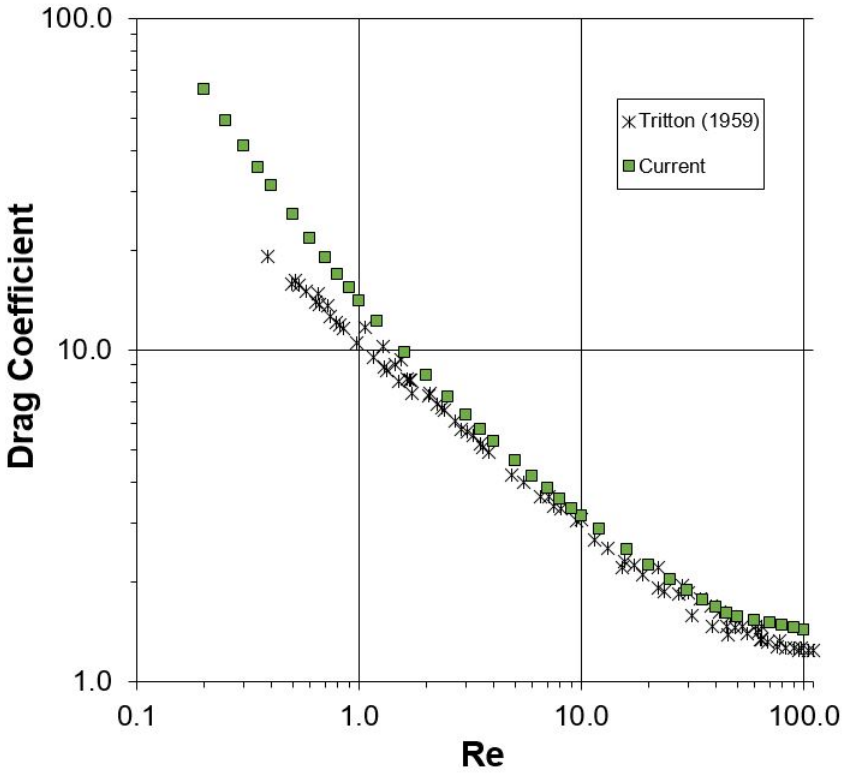

Figure 4.1: Newtonian drag results for inertial flow at low Re.

A notable feature of the Newtonian simulation, however, was the numerical instability and lack of convergence. Firstly, the model became increasingly unstable as the grid size was increased, with the range of viscosity which attained a stable solution decreasing; above and below certain viscosities, an unstable solution was observed. This behaviour was exaggerated at high Re. Secondly, the model failed to converge to a single solution for large grid sizes, independent of the Reynolds number. Hence, in order to attain numerical stability and adequate convergence, a grid size of 640×640 cells was used for all simulations. Consequently, while maintaining a domain size of $W/d = 16$ to minimise wall effects, this lack of achievable grid resolution significantly influenced the drag results.

Next, the flow of a Bingham fluid past the same 2-D cylinder was analysed for the TRT and IR models. For simulations utilising the TRT model, however, inconsistencies in the drag became evident. Figure 4.2 displays the variation of the drag with changing viscosity obtained with both the IMB and BB boundary formulations of the TRT model, as well as that of the IR model with IMB, at constant fluid conditions of $Bi = 5$ and $Re = 0.1$. Clearly, the TRT-obtained drag was dependent on the prescribed viscosity of the viscoplastic fluid, a phenomenon which should not be observed for constant Bi and Re. Importantly, the IR-IMB model appears to show the correct constant drag; in reality, the results differ by 3.4% between the highest and lowest viscosities tested for the IR model, however drag converges as viscosity is decreased. For viscosities above and below those plotted, the simulations became unstable. Notably, the BB method for the TRT model converged with decreasing viscosity within the stable range, while convergence of the IMB formulation is questionable with such significant variations in drag results. It must also be noted that, in addition to the very small stable viscosity range of the TRT-BB model, convergence of the simulations was poor at small viscosities. A decreased grid size was required for the TRT-BB simulation to ensure convergence. For example, compared to the 1024×1024 grid with a 64 cell sphere diameter used for the IR simulations, the resolution was decreased to 192×192 with $d = 24$ cells for the TRT-BB model.

In addition to the viscosity dependence, stability and convergence issues of the TRT formulation presented above, Figure 4.2 demonstrates that the TRT-BB simulation significantly over predicted the drag obtained by the IR-IMB model. Proving the accuracy of the present implicitly-regularised LBM-DEM model, Table 4.1 compares the drag obtained over a range of Re and Bi by the IR-IMB model to results in the literature. In light of the small viscosity dependence discussed above, a viscosity equal to 0.032 lattice units was used for all tests.

For the implicit regularisation, the convergence characteristics of using each the BB and IMB formulations to model interaction at the cylinder-fluid interface were also analysed. Figure 4.3 depicts the convergence of the drag results with increased grid refinement at $Re = 10$ and $Bi = 5$.

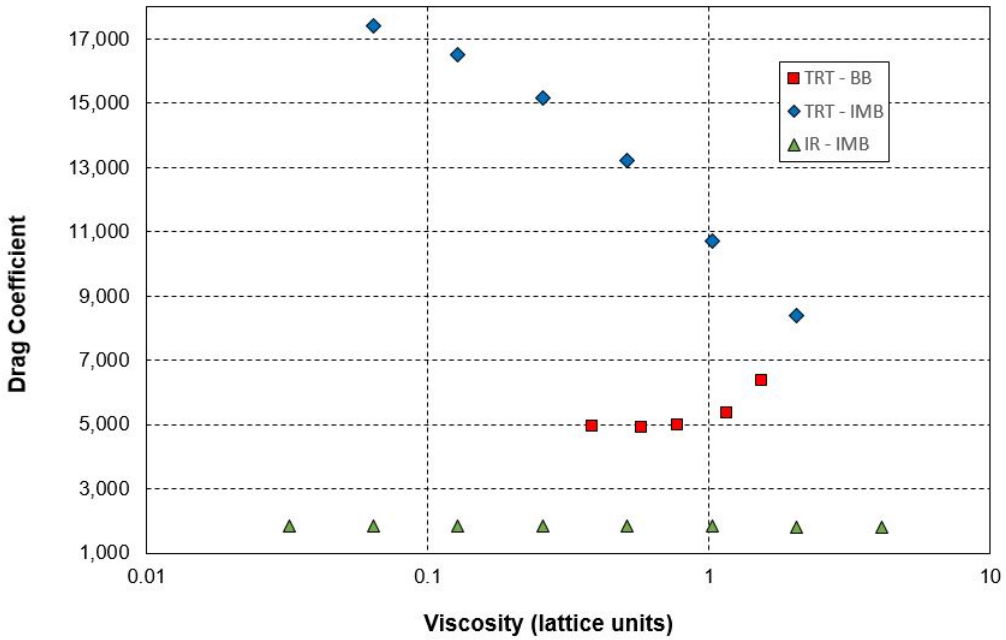

Figure 4.2: Dependence of the drag obtained by the TRT-IMB model on fluid viscosity, compared to the BB boundary formulation.

Table 4.1: Drag results for the flow of a Bingham fluid past a 2-D cylinder obtained by the present TRT (with BB) and IR (with IMB) LBM-DEM models.

	$Bi = 1$		$Bi = 5$		$Bi = 10$	
Re	IR	[15]	IR	[15]	IR	[15]
0.1	592.58	598.21	1867.0	1950.1	3281.4	3308.8
10	6.6376	6.8994	19.268	19.405	33.272	33.105
20	3.8306	3.9749	10.128	10.192	17.087	16.996
40	2.4004	2.4262	5.5307	5.5597	9.0215	8.9614

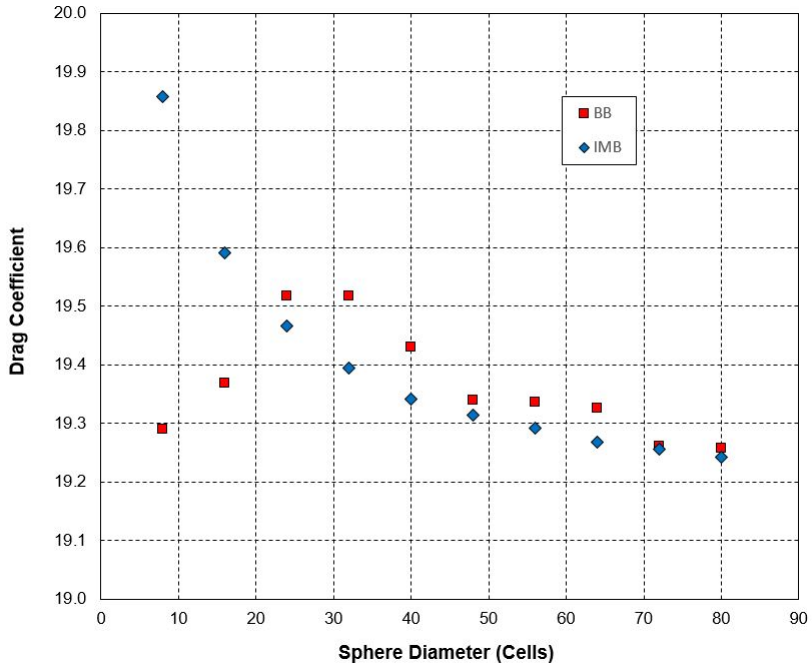

Figure 4.3: Comparison of grid refinement (represented by the number of cells utilised for the sphere diameter) convergence between BB and IMB cylinder boundary formulation.

4.1.1.1 Vortex Shedding

When analysing vortex shedding, the non-dimensional Strouhal number, St, is used to quantify the transient flow properties behind the object in question. For a cylinder of diameter D,

$$St = \frac{fD}{U}, \tag{4.1}$$

where f is the frequency at which vorticies are shed and U is the flow velocity past the cylinder. For this investigation, the shedding frequency utilised was for each single vortex, irrespective of whether it was shed at the top or bottom of the cylinder.

While the effect of Re on St for Newtonian flows has been extensively studied, no literature results currently exist for vortex shedding in Bingham fluids. Hence, the following aims to quantify the effects of the Bingham number on the characteristics of vortex shedding past a single cylinder.

Table 4.2 depicts the variation in the Strouhal number, as well as the time taken for the onset of transient flow to occur (in thousands of lattice units), as τ_y was increased at $Re = 160$. A temporal resolution of 50 lattice time units was used when determining the vortex shedding frequency, resulting in an accuracy of St to approximately two significant figures.

Table 4.2: Variation of St and transient flow onset times ($t_{transient}$) for increasing Bi at $Re = 160$.

Bi	St	$t_{transient}$ ($\times 10^3$ lattice units)
0	0.42	8
0.2	0.42	9
1	0.38	10
2	0.36	21

A clear decrease in St, corresponding to a decrease in shedding frequency, occurred as Bi was increased. The flow remained in a steady state for a period before the onset of transient flow, which occurred later as Bi was increased. Interestingly, when the cylinder centre was positioned exactly halfway along the domain width (rendering the solution symmetric), the onset of transient flow occurred much later compared to the case where the cylinder was offset from the centre by a distance of 0.1 cells. This offset was representative of a real-world solution, in which symmetric flows never occur. Figure 4.4 displays the flow development at $Bi = 2$ for the symmetric and offset simulations. The development of a full von Karman vortex street is evident. For Bi larger than approximately 2.7 - 2.8 vortex shedding did not occur.

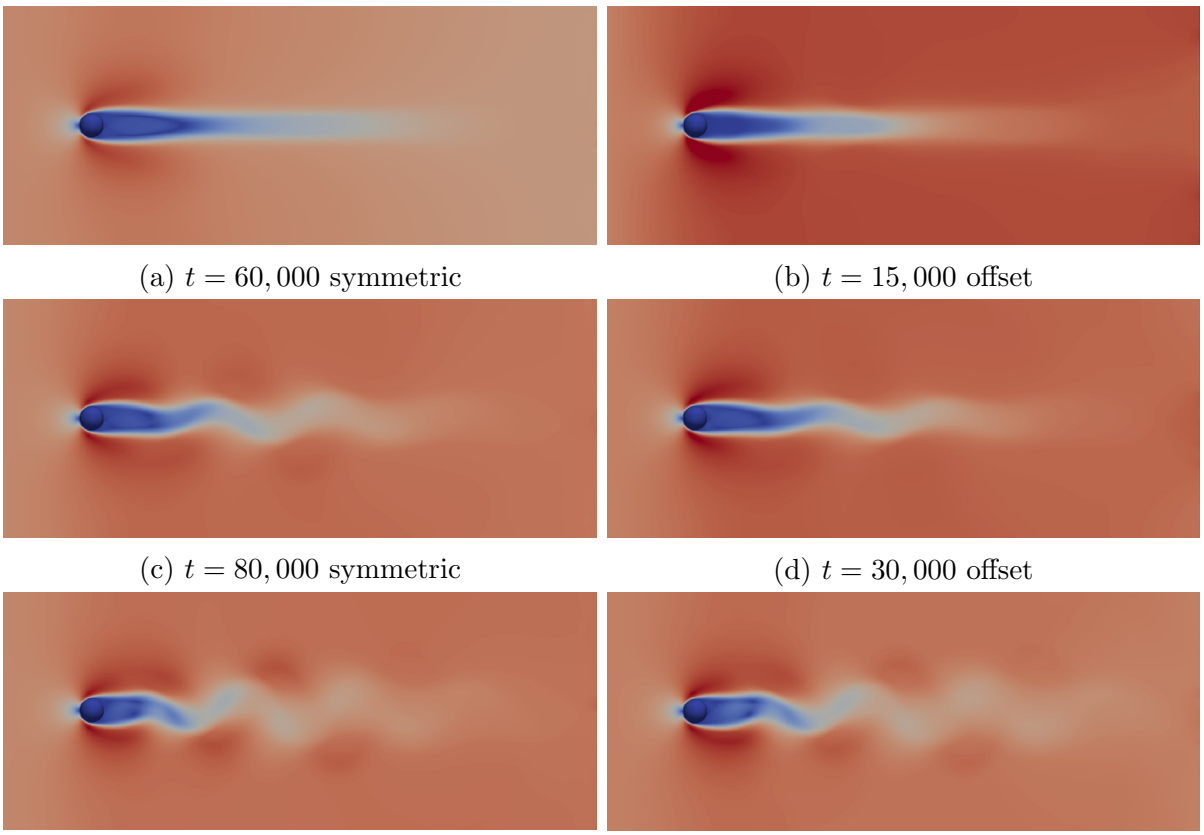

(a) $t = 60,000$ symmetric

(b) $t = 15,000$ offset

(c) $t = 80,000$ symmetric

(d) $t = 30,000$ offset

(e) $t = 100,000$ symmetric

(f) $t = 45,000$ offset

Figure 4.4: Development of vortex shedding over lattice unit time, t, for symmetric and offset simulations at $Bi = 2$ and $Re = 160$.

4.1.2 Periodic Cylinder Array

Increasing the complexity of the validation, the drag force imparted on a periodic array of cylinders by a Bingham fluid was measured. Over a range of Bi and array porosities, ϕ, the Newtonian drag coefficient was subtracted from the measured drag coefficients. Figure 4.5 compares the measured drag results obtained by the IR model against data originally published by Spelt et al. [16].

Investigating the upper bounds of stability, utilising the domain length as the characteristic length, the solution became unstable at a cell averaged velocity of approximately 0.34 - 0.35 (in lattice units) for Newtonian flow, irrespective of the Reynolds number of the flow. Significantly, the implicitly regularised model remained stable for Bi effectively up to infinity in both creeping and inertial flow.

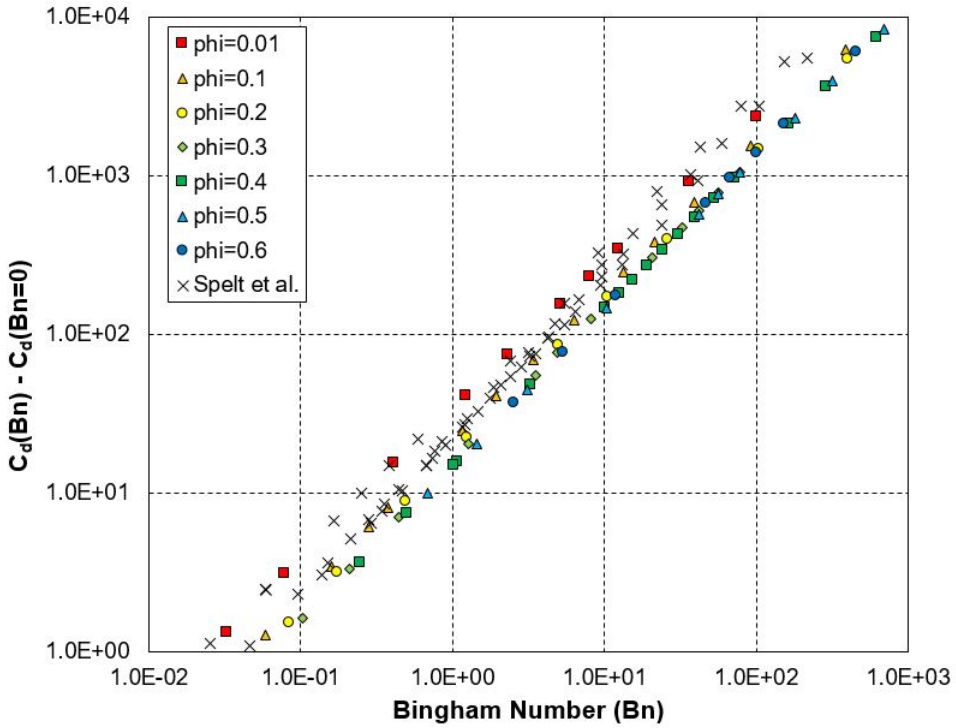

Figure 4.5: Bingham fluid C_D obtained by the IR model, normalised against Newtonian C_D as a function of Bi, compared to data originally published by Spelt et al. [16].

4.2 Validation in Three Dimensions

4.2.1 Creeping Flow

The effects of increasing the yield-stress of a Bingham fluid on the flow around a particle were analysed for comparison to documented studies in the literature. Figure 4.6 depicts the yielded (grey) and un-yielded (black) regions of creeping fluid surrounding a sphere for increasing Bi obtained by the IR model.

Quantifying these creeping flows, the drag force acting on the sphere was calculated over a range of Bi. Initially, however, domain independence and grid sensitivity analyses were conducted in order to quantify any error associated with wall and grid resolution effects respectively. The IR model was used throughout these analyses. Figure 4.7 depicts the convergence of C_S as H/d was increased for $Bi = 1$ and 100.

For low Bi, wall effects became negligible for $H/d \geq 6$, with the drag converging to a 0.01% error relative to the domain-independent solution. For the increased yield-stress, however, C_S failed to converge to three significant figures up to $H/d = 12$, at which point the limit of computational memory was reached.

The grid sensitivity analysis was performed at $H/d = 6$ for both $Bi = 1$ and 100 to allow for sufficient convergence with the available computing memory, recognising that wall effects were present in the analysis at $Bi = 100$. Figure 4.8 illustrates second order solution

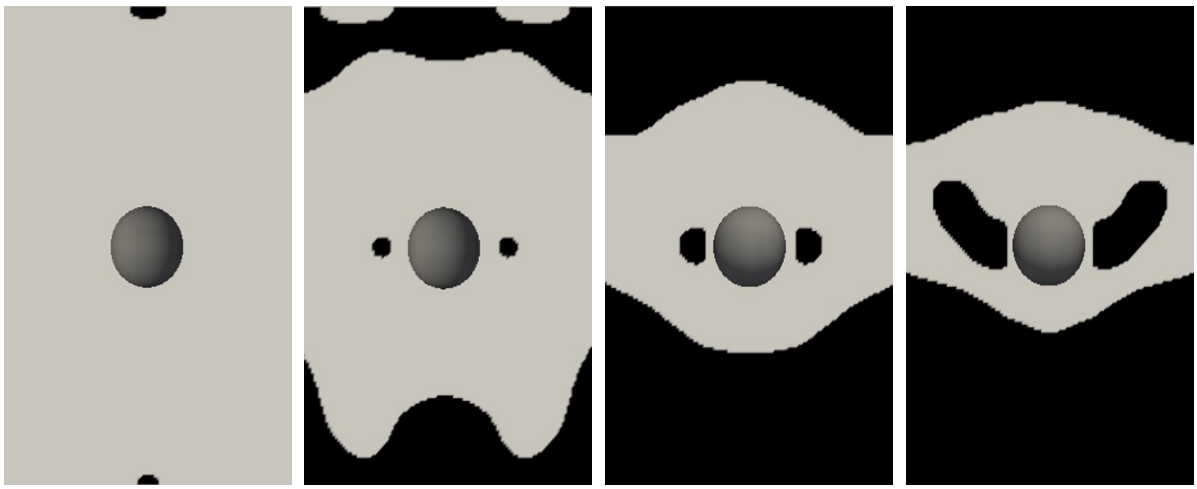

(a) $Bi = 0.1$ (b) $Bi = 1$ (c) $Bi = 5$ (d) $Bi = 10$

Figure 4.6: Yielded (grey) and un-yielded (black) regions of creeping flow around a fixed sphere predicted by the LBM-DEM IR model for increasing Bi (flow from bottom to top). $6 \times 4 \times 4$ ($L/d \times H/d \times H/d$) of a larger $6 \times 10.6 \times 10.6$ domain is shown, which was used to minimise wall effects.

convergence for increased grid refinement. For $Bi = 1$, C_S converged to four significant figures at $d = 40$ (representing the maximum resolution achievable with the available memory), and was deemed as the zero-error solution for the purpose of comparison to the values in the literature. For $Bi = 100$, however, the solution failed to converge to three significant figures with the available computing memory. Interestingly, the drag was overestimated for $Bi = 1$ but underestimated for $Bi = 100$ at low grid resolutions.

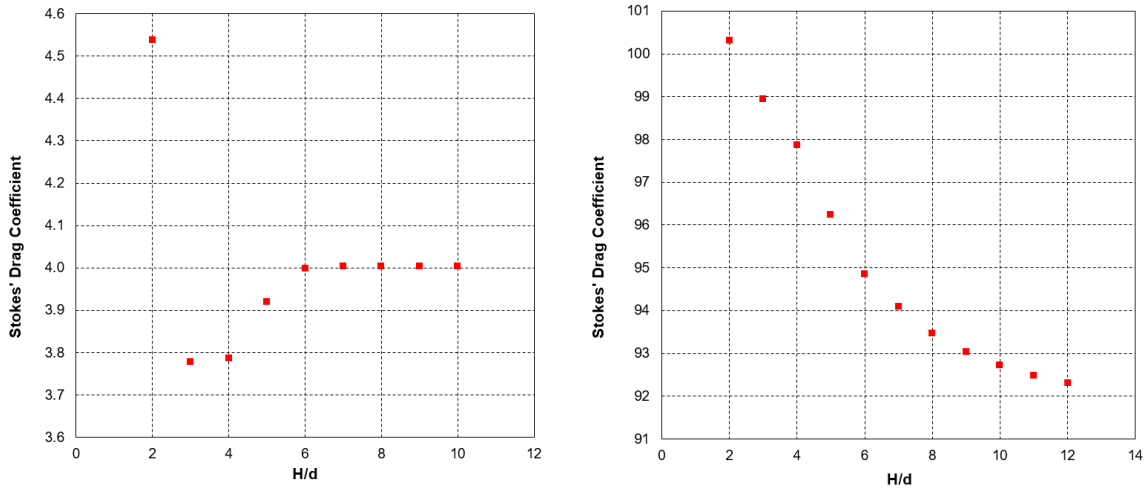

(a) (b)

Figure 4.7: Dependence of drag on sphere diameter-to-domain height ratio, H/d, for (a) $Bi = 1$ and (b) $Bi = 100$.

Hence, it was deemed pertinent to utilise $d = 40$ and $H/d = 6$ for all tests. For $Bi < 1$, no error was therefore present in the result. For high Bingham numbers, however, it was expected that the model would increasingly underestimate C_S as Bi was increased.

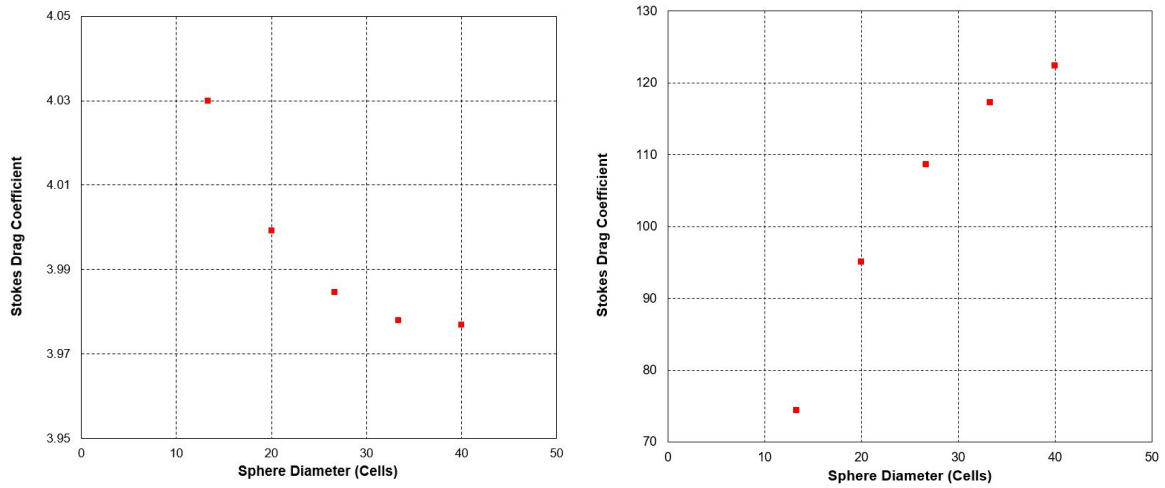

(a) (b)

Figure 4.8: Dependence of drag on grid resolution for fixed sphere in square based, rectangular domain for (a) $Bi = 1$ and (b) $Bi = 100$.

When simulating the fixed sphere scenario utilising the TRT model, however, similar viscosity-dependant behaviour to that of the TRT-IMB cylinder case was observed. Although to a lesser extended than the 2-D scenario, Figure 4.9 illustrates a clear dependence of the drag on the fluid's viscosity for creeping flow at constant Bi. The model became unstable for viscosities above and below those plotted.

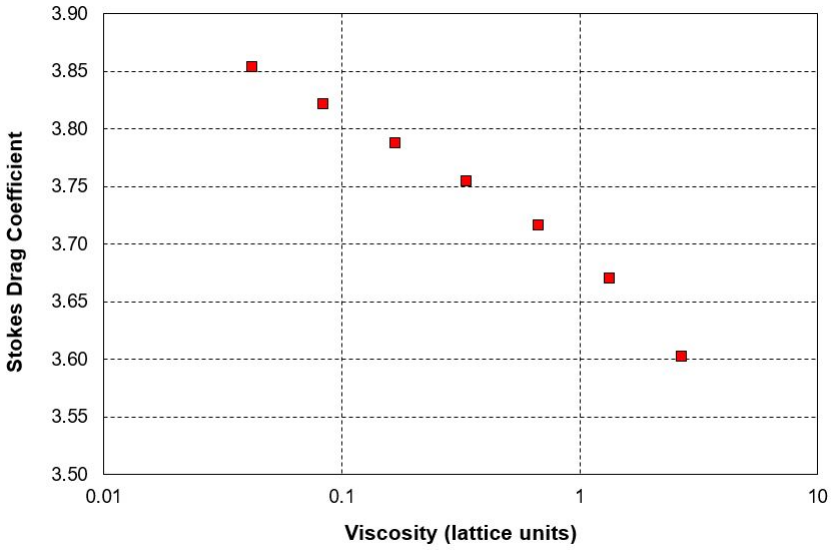

Figure 4.9: Variation of C_S with fluid viscosity for creeping flow past a fixed sphere utilising the TRT model at $Bi = 1$.

Seeing as the C_S obtained by the TRT approached the IR solution as viscosity was decreased, the lowest viscosity possible while retaining numerical stability was used for all 3-D TRT simulations. Table 4.3 lists the Stokes drag coefficients obtained by the IR and TRT models over a range of Bi for creeping flow past a fixed sphere, juxtaposed with those from a prominent numerical study.

Table 4.3: Comparison of present C_S values for creeping flow past a fixed sphere obtained over a range of Bi to those in the literature [10, 12].

Bi	Present (TRT)	Present (IR)	Liu et al. (2002)
0.007	1.31	1.26	1.16
0.108	1.64	1.59	1.74
0.747	3.21	3.43	3.45
2.299	6.11	6.36	6.38
8.047	15.05	15.07	15.21
14.91	24.34	24.43	24.85
27.36	40.06	40.43	41.46
59.59	77.53	79.03	82.67
197.5	-	182.87	252.6
340.7	-	223.01	426.0
544.6	-	247.29	671.9

4.2.2 Settling Sphere

As described in the methodology, moving on from fixed sphere validation, a settling sphere in a domain containing a stationary Bingham fluid was analysed. Initially, the yielding limit was observed, with the gravitational-to-yield force parameter, Y_G, quantifying the limit at which the particle would overcome yield-stress forces and begin to exhibit motion. Table 4.4 compares the Y_G obtained via the TRT (at a viscosity of 0.01 lattice units) and IR LBM-DEM models to those by prominent experimental and numerical studies.

Table 4.4: Comparison of the gravity-to-yield parameter, $Y_{G,crit}$, obtained by the current implicitly regularised LBM-DEM model to literature values.

Study	$Y_{G,crit}$
Present - TRT	0.062
Present - IR	0.049
Ansley & Smith (1967)	0.068 - 0.084
Beris et al. (1985)	0.048
Atapattu et al. (1986)	0.095 - 0.111
Blackery & Mitsoulis (1997)	0.048
Merkak et al. (2006)	0.062 - 0.088
Chen et al. (2016)	0.046

Allowing the particle to settle, the terminal drag force acting on the settling sphere was measured, such that the hydrodynamic drag induced by a Bingham fluid in an inertial flow was compared to prominent existing numerical and experimental data. The inertial, viscous and yield-stress properties of the flow were characterised by the non-dimensional modified Reynolds number, Re^*. Before collating data, however, a grid sensitivity analysis, independent to that of the fixed sphere scenario, was undertaken.

To investigate the effect of grid resolution, the test conditions were initialised with $Re^* \approx 1 - 2$, such that the sphere experienced low inertial effects, requiring a tube-to-sphere diameter ratio, D/d, of 6 to ensure that wall influences were negligible. Additionally, at this low Re^*, the correlations developed between C_D and Re^* in the literature (Equations 2.11 and 2.12) had a high degree of accuracy. Hence, in quantifying the simulation error, the difference between the measured C_D and the corresponding experimentally and numerically correlated values were calculated. Figure 4.10 depicts a clear convergence of the drag results with increasing grid resolution.

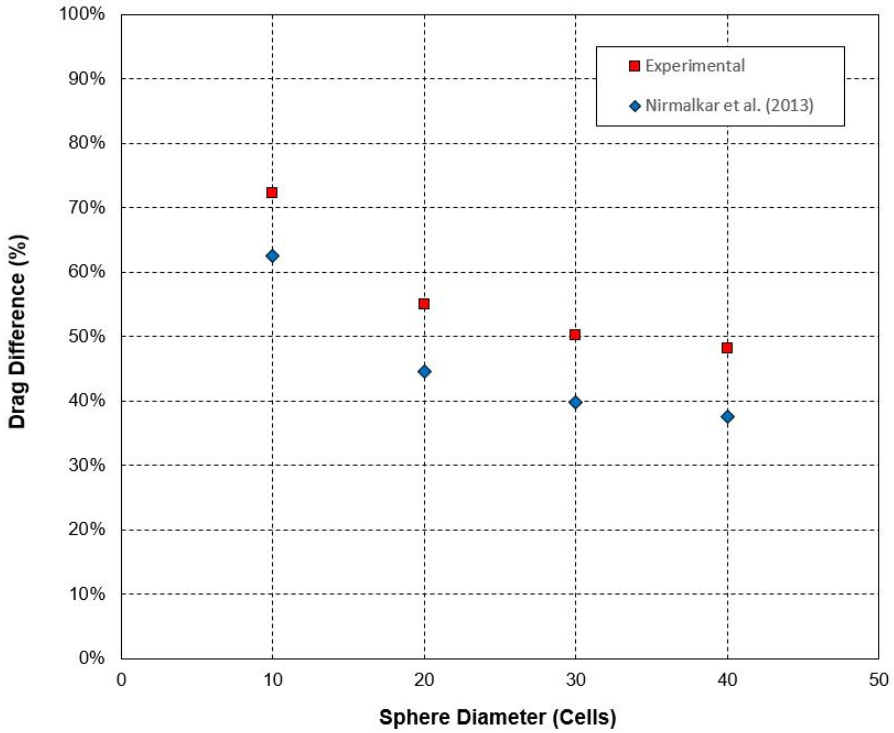

Figure 4.10: Difference between measured drag coefficients and those predicted by numerical and experimental literature studies for increasing grid resolutions. Study performed at $D/d = 6$.

As previously discussed, the available computing memory presented a limitation to the grid resolution, requiring a trade off between resolution and domain size. At low Re^*, domain size was not an issue, with sufficient tube width to negate any wall influences and sufficient length to ensure the particle reached its terminal velocity without the bottom floor influencing the flow. As Re^* was increased, however, the height of the tube quickly

became a problem, with the sphere requiring a longer distance to reach its terminal velocity.

Hence, for the purpose of comparison to the literature data, it was deemed pertinent to utilise $d = 30$ cells and $D/d = 6$ to allow sufficient tube length for the sphere to settle, minimise wall effects, and minimise resolution-associated error, recognising the inaccuracies associated with these. Figure 4.11 displays the drag results over $0.001 < Re^* < 100$ obtained by the TRT and IR models, as well as the zero yield-stress Newtonian solution, compared to those of prominent literature studies.

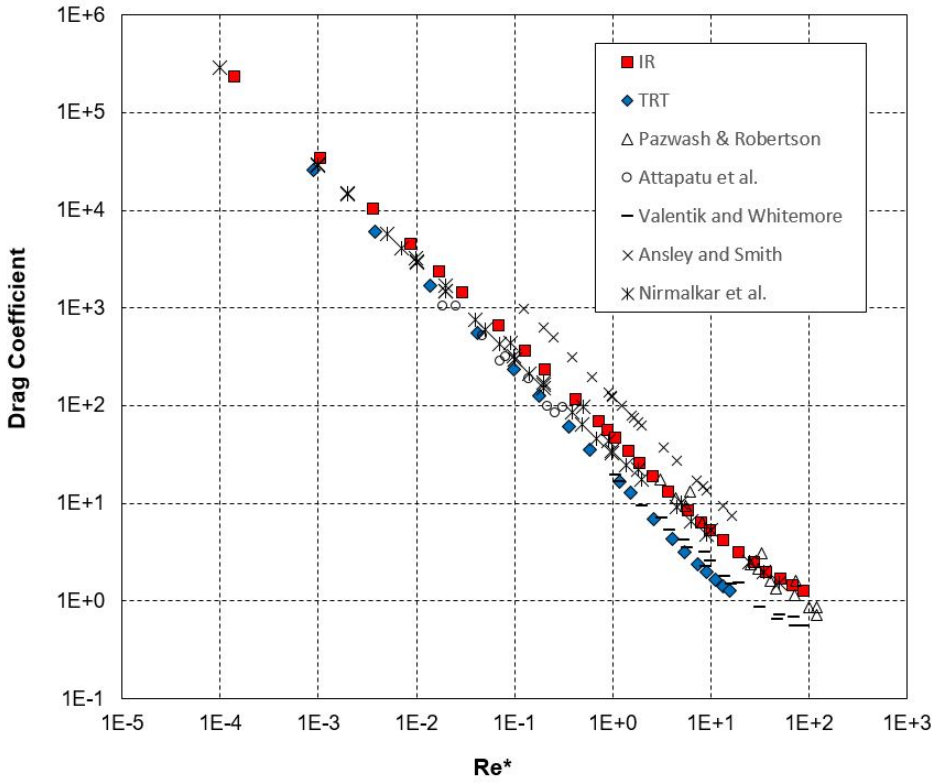

Figure 4.11: C_D for a sphere settling in a slip tube over a range of inertial and yield-stress conditions, compared to prominent literature and experimental studies [20–24].

4.2.3 Co-Linear Interacting Spheres

In observing hydrodynamic interactions between particles, Figure 4.12 depicts the drag variation with sphere separation distance over a range of Bi.

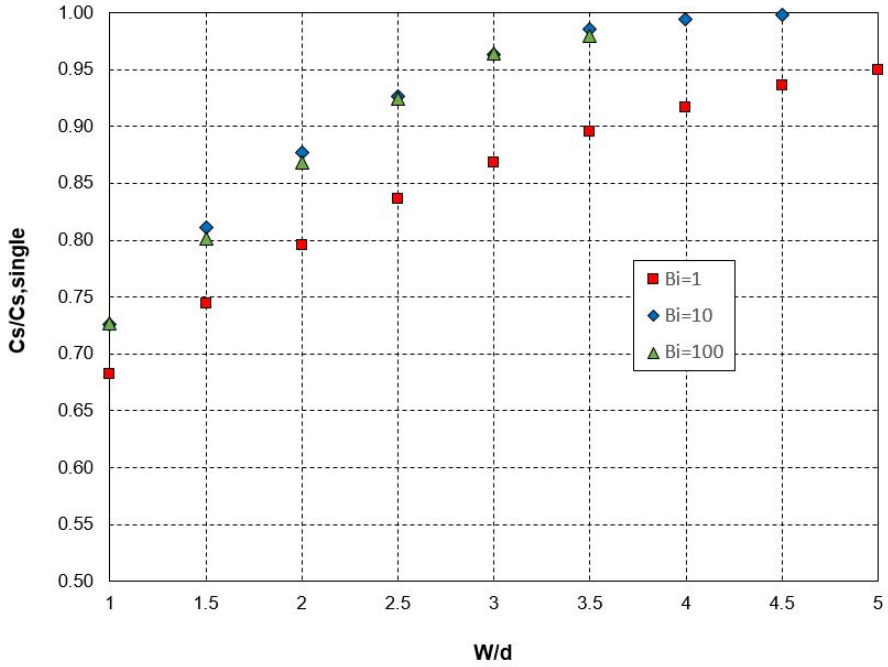

Figure 4.12: Variation of drag for fixed co-linear spheres with increasing sphere separation distance, represented by $C_S/C_{S,single}$ and W/d respectively, at various Bi.

For qualitative comparison of the yielding behaviour between the spheres to the literature results, Figure 4.13 illustrates the regions of yielded (grey) and un-yielded (black) fluid surrounding the particles at varying Bi. Similarly, Figure 4.14 shows the variation in static fluid as the sphere separation distance was increased at constant Bi.

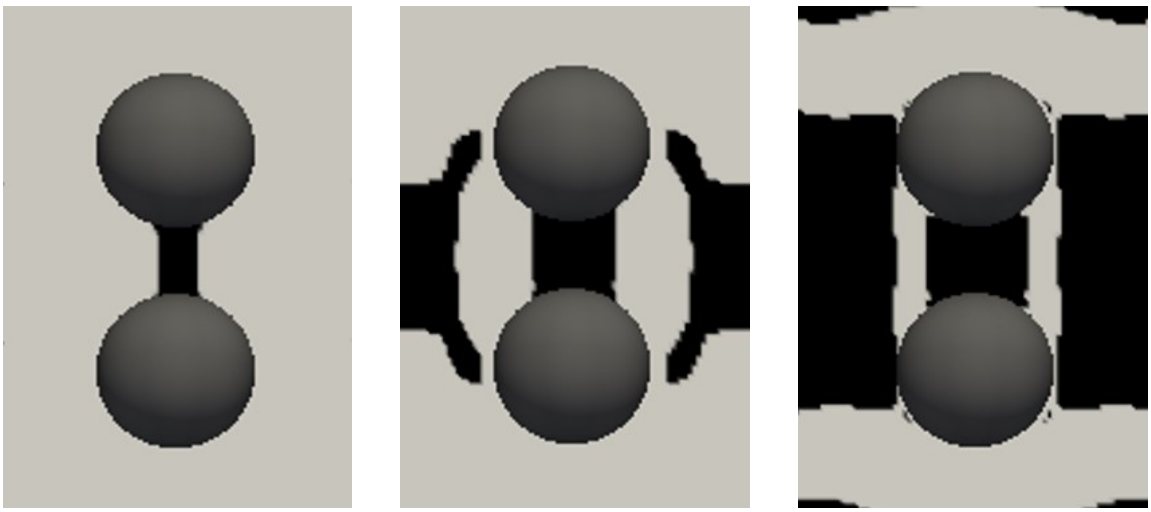

(a) $Bi = 1$ (b) $Bi = 10$ (c) $Bi = 100$

Figure 4.13: Variation of un-yielded region (black) connecting two spheres translating co-linearly for increased Bi.

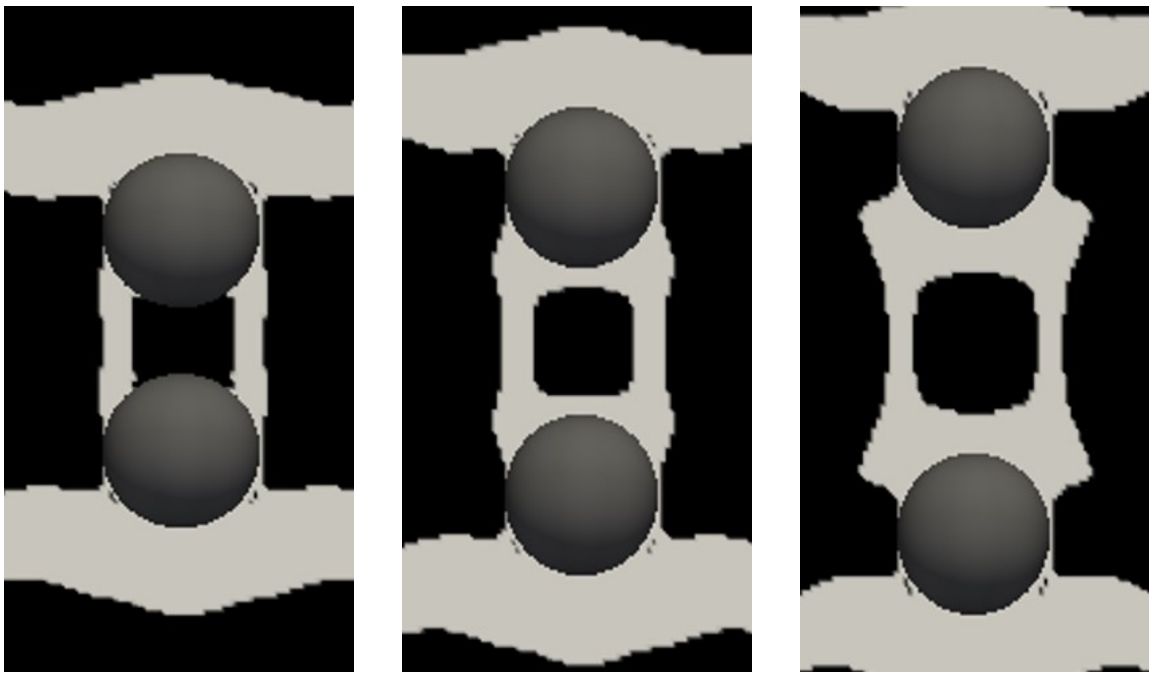

(a) $W/d = 1.5$ (b) $W/d = 2$ (c) $W/d = 2.5$

Figure 4.14: Variation of un-yielded region (black) connecting two spheres translating co-linearly for increasing separation distances at constant Bi.

Chapter 5

Analysis and Discussion

5.1 Two-Dimensional Single Cylinder

5.1.1 Newtonian Flow

Referring to Figure 4.1, the Newtonian drag results obtained in low inertial flow matched the literature data reasonably well over the range $1 < Re < 50$. Rather than exhibiting a linear log-scale correlation between C_D and Re for low Re, however, the drag began to deviate noticeably from that presented in the literature. This discrepancy at low Re, where viscous effects dominated inertial effects, suggested possible inaccuracies in the modelling of the viscous forces present in fluid-solid interactions. However, as previously discussed, the lack of grid resolution and domain size attainable while retaining numerical stability most likely contributed to some of the deviation. The disparity at high Re can likewise be attributed to this. This behaviour shall be monitored and investigated further when analysing the Bingham fluid results for creeping flow in the 2-D and 3-D scenarios.

5.1.2 Comparison of Two-Relaxation-Time model and Implicitly-Regularised model for Bingham Fluids

Moving on to Bingham fluid flow, as discussed in detail in Section 4.1.1, significant issues in the TRT model were identified. Firstly, both the IMB and BB boundary formulations were highly viscosity dependent. As discussed in the Literature Review, the TRT model operates with a Papanastasiou regularisation. Essentially, at low strain rates, the fluid is treated as highly viscous. When coupled with the kinetic nature of the LBM, in which the relaxation parameter is linked to the fluid viscosity, inaccuracies are highly likely, presenting a very likely explanation for the viscosity dependent behaviour. Furthering this, while the BB simulations converged to a constant drag value as viscosity was decreased, the TRT-IMB model displayed no obvious convergence with viscosity. This suggests that

the IMB formulation manifests the problem of viscosity and relaxation rate dependence, a statement which is rendered plausible considering the IMB's modification of the LBE.

While numerous issues arose with the Papanastasiou regularised TRT model, the results obtained for flow past a 2-D cylinder with the IR model matched the literature results very closely. Referring to Table 4.1, an average and maximum difference between the present and literature results of 1.51% and 4.26% respectively was observed. Considering that the literatures study's drag solutions were obtained utilising a PR finite element method, these results were considered to be in close correlation. The only notable inaccuracy of the IR model was in the small dependence on viscosity, quantified as a 3.4% difference between the highest and lowest viscosities tested.

Interestingly, and indeed very importantly, the lack of convergence and numerical instability observed in the Newtonian simulations were not present for these Bingham flow solutions. Overall, it can be concluded that the present IR LBM-DEM model was validated for and was successful in modelling Bingham fluid interactions with single 2-D particles.

In terms of the characteristics of the bounce-back and immersed-moving-boundary methods for the modelling of the fluid and stationary cylinder interface in the IR model, Figure 4.3 depicts clear 2nd-order convergence of the IMB solution with increased grid resolution. The BB method, however, exhibited no discernible trend in convergence. While it appeared to eventually converge to the IMB solution, the drag solution for lower refinements was overestimated for resolutions of greater than 20 cylinder diameter cells. In three dimensions, this error is magnified, due to the increased number of cells with fluid-solid interfaces. Hence, while the real power of the IMB method lies in the modelling of moving boundaries, this demonstrates its superiority over BB for the modelling of curved stationary particle boundaries.

5.2 Periodic Cylinder Array

Figure 4.5 displays a linear correlation on the log-log scale between cylinder drag and Bi for Bingham flow through a periodic array of cylinders attained by the current implicitly regularised LBM-DEM. This trend was also observed by Spelt et al., albeit with consistently higher drag, with the discrepancy becoming larger at high Bi. It is postulated, however, that the current IR model obtained a more accurate solution of the yield-stress compared to the bi-viscosity regularised numerical literature study, especially at higher Bi, where the divergence between results increased.

Additionally, the significant increase in drag at a very low solid area fraction observed by Spelt et al. was replicated. It is suggested that at this high porosity, the increase in drag resulted from greatly decreased flow interaction between the cylinders, suggesting

accurate modelling of inter-particle hydrodynamic effects for the 2-D scenario. A low sphere resolution can be discounted as the cause due to the near exact same results obtained by Spelt et al.

5.3 Three-Dimensional Validation

5.3.1 Creeping Flow

Referring to Figures 2.5 and 4.6, the IR LBM-DEM model recovered a number of the flow features documented in the two LBM-DEM literature studies. Of particular importance were the regions of un-yielded flow to either side of the sphere. In three dimensions, these regions corresponded to a solid ring of un-yielded fluid surrounding the sphere, as visualised in Figure 5.1. Like the MRT model from the literature, the rings became evident at approximately $Bi = 1$ using the current implicit regularisation, while the bi-viscosity model from the literature did not predict ring formation until $Bi = 5$. Additionally, the rings became larger as the Bingham number was increased.

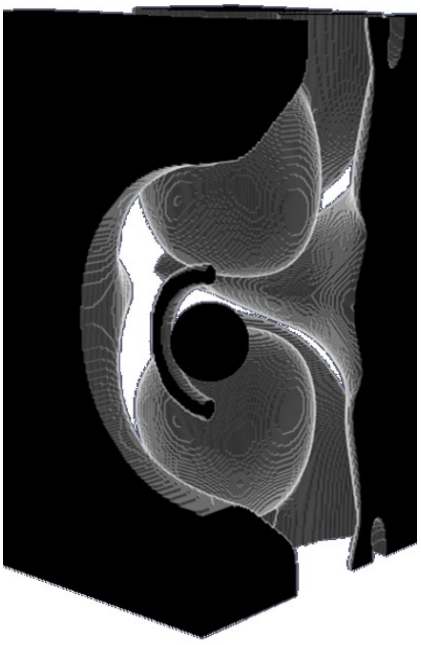

Figure 5.1: 3-D representation of the yielded (clear) and un-yielded (solid) regions for creeping flow past a fixed sphere at $Bi = 1$ predicted by the IR model. A quarter of a $10 \times 8 \times 8$ domain is shown, with flow from front-left to back-right.

However, unlike the constant velocity walls implemented in the previous studies, which rendered the flow symmetric around all axes, slip walls were utilised in this investigation for the simplicity of their implementation. Hence, while the flow exhibited symmetry about the longitudinal axis, the shape of the yielded regions before and after the sphere were asymmetric due to interactions at the domain wall.

A feature of the documented flows which was not in evidence in the current model were the solid caps formed at the poles of the sphere for high Bi. It is impossible to say whether the lack of these regions were an inherent prediction of the IR model or, as mentioned above, a symptom of the wall effects. Hence, in order to provide a better comparison to the literature, it is recommended that the domain is constructed with constant velocity walls for a more thorough future comparison.

As Bi was increased, the un-yielded region also increased in size, with the yielded region experiencing diminishing to no interaction with the domain walls. Interestingly, referring to the domain dependence plots at $Bi = 1$ and 100 (Figure 4.7), the lower yield-stress flow was less affected by wall interactions than at the higher Bi, suggesting that the domain walls affected the sphere drag to a greater degree when interacting with un-yielded fluid in bulk-motion.

5.3.1.1 Performance Comparison of Two-Relaxation-Time model and Implicitly-Regularised model

The drag results for a sphere in a creeping Bingham flow, presented in Table 4.3, provided further corroboration to the characteristics exhibited in the qualitative flow-field visualisations. For low Bi, the C_S obtained by the IR model closely matched the values from the literature. As Bi increased, however, the simulated values became significantly lower. As documented in the results, however, this arose due to an inadequate mesh refinement, caused by a lack of available computational memory. Unfortunately, this also hindered any ability to investigate the accuracy of the regularisation parameters used in the Papanastasiou-regularised literature studies, which decreased significantly at high Bi in order to ensure numerical stability. Overall, the similarity between the literature and IR-obtained results provides further evidence that the implicit regularisation is successful in modelling viscoplastic fluid-particle coupling.

When applied to the 3-D fixed sphere simulation, the TRT model exhibited the same viscosity dependent behaviour seen in the 2-D scenario. Interestingly, however, the drag was significantly less dependent on the fluid viscosity as compared to the 2-D cylinder simulation. This improved performance was also noticed when the model was subjected to a range of Bi in the creeping flow regime. As presented in Table 4.3, the drag obtained by the TRT model matched the IR and literature results reasonably closely. If anything, drag was consistently underestimated, a trend which shall be noted in subsequent simulation results.

5.3.2 Settling Sphere and Inertial Flow

A key indicator of a numerical model's ability to correctly model the yield-stress of a fluid is the replication of the yielding-point phenomena of a single sphere. Significantly, the

IR LBM-DEM exactly observed, in relation to existing numerical results, the gravity-to-yield parameter value at which the gravitational force acting on the sphere overcame the resisting yield-stress. The TRT model, however, significantly overestimated the critical yield-stress in relation to the literature and IR results. This suggests that the explicitly solved TRT method predicted over-yielding of the fluid which, as hypothesised, was most likely due to the implementation of the Papanastasiou regularisation.

Referring to Figure 4.11, the drag on the settling sphere obtained with implicit-regularisation was in excellent agreement with that of Nirmalkar et al. Two key features of the data indicated that the effects of the yield-stress, viscous and inertial forces were correctly modelled: at low R^e*, where yield-stress forces dominated, the linear inverse trend between C_D and Re^* was replicated; at high Re^*, the Bingham drag results converged to the Newtonian solution, where inertial forces were much larger than those imparted by the yield-stress and viscous components of the flow. If anything, the drag observed by the current model was slightly higher than the numerical literature results. The spread of experimental results between studies is quite large, owing to error induced by both the use of finite-sized tubes and the difference in the evaluation methods of the fluids' τ_y between studies. However, as with the data of Nirmalkar et al., the IR-obtained results can be concluded to reflect the main features of these experimental drag results.

The TRT model, on the other hand, diverged significantly from the numerical and experimental literature results at high Re^*, suggesting that the accuracy diminishes when large inertial effects are present. For $Re^* < 1$, however, the data is in excellent agreement with that from the literature. This is in line with the fixed sphere results, in which the TRT model accurately predicted the drag at very low Re (in the creeping flow regime). As also observed in the fixed sphere simulation, the drag was consistently lower than the literature and IR results, leading to the final conclusion that the Papanastasiou regularisation predicted over-yielding over the fluid.

5.3.3 Inter-Particle Hydrodynamic Effects

Firstly, Figure 4.12 clearly depicts the interaction effects of the two spheres, with the two-sphere drag approaching the single sphere drag solution ($C_S/C_{S,single} = 1$) with increasing separation distance. Significantly, the separation distance at which sphere interactions ceased increased as the Bingham number of the flow decreased, approaching the Newtonian solution. This result was also observed in the literature, albeit for a single Bingham number compared to the Newtonian solution.

Notably, no difference in interaction effects between $Bi = 10$ and $Bi = 100$ were observed. While this suggests a limiting value for a yield-stress above which interaction effects become constant, the grid refinement study presented in Section 4.2.1 indicated a large underestimation of the drag for inadequate grid resolutions at $Bi = 100$. Therefore, while

the conclusion of an interaction plateau above a certain τ_y is most likely correct, the drag for $Bi = 100$ in Figure 4.12 can be assumed to be underestimated compared to the grid independent solution.

As illustrated in Figure 4.13, a non-yielded region connecting each sphere was observed for spheres in close proximity, which is consistent with observations in the literature. This region clearly increased in size as the Bingham number was increased. Interestingly, however, this increase in un-yielded fluid did not correspond to an increase in drag between $Bi = 10$ and $Bi = 100$, as discussed above. As also depicted in past results and presently illustrated in Figure 4.14, this un-yielded plug detached from the spheres as the separation distance was increased. A 3-D representation of this occurrence is shown in Figure 5.2, clearly depicting the solid, detached plug between the particles.

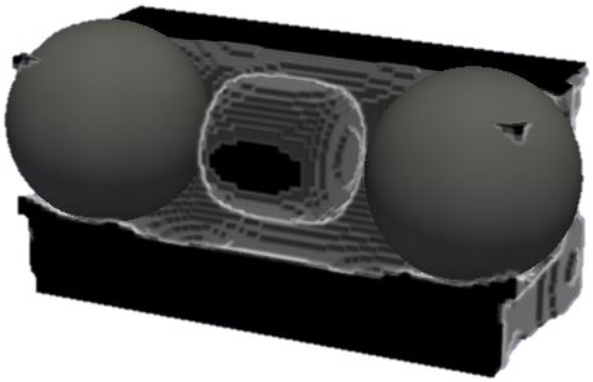

Figure 5.2: 3-D representation of the un-yielded plug formed between two interacting spheres at $Bi = 100$, $W/d = 2$.

Overall, these qualitative and quantitative results are highly agreeable with those previously documented for the interaction of two spheres in a Bingham fluid, providing a final piece of evidence to validate the present implicitly-regularised model's ability to model yield-stress fluid-particle interactions.

Chapter 6

Conclusions and Recommendations

The use of dense viscoplastic fluid-particle suspensions has recently seen a large increase in novel industrial applications such as hydraulic fracturing and long distance pipeline particulate transport. In order to maximise the success of these processes, complete characterisation of the suspensions' rheological behaviours is critical. However, as of now, no comprehensive modelling strategies exist for the suspensions as a whole. In addition to the problem of continuously updating particle boundaries, classical CFD methods, and indeed any attempt at numerically modelling viscoplastic fluids, encounter significant complexities caused by the presence of a yield-stress. Currently, a number of explicit regularisation techniques are used to approximate the yield-stress, the inherent numerical inaccuracies of which are quite often given little attention.

A coupled LBM-DEM numerical approach presents an excellent solution to modelling the bulk movement of particles within suspensions, and has been successfully applied to the modelling of dense Newtonian suspensions. Of key importance, however, the LBM allows for an implicit regularisation of the yield-stress, in which the constitutive Bingham fluid is solved without the need for the approximations of current explicit solvers. Hence, it was hypothesised that the implicitly-regularised (IR) model is superior for the modelling of viscoplastic fluids, a claim which, if true, would lead to the eventual direct numerical simulation of dense viscoplastic particle suspensions.

In total, five test configurations were developed to validate the present IR model, evaluate its suitability for characterising viscoplastic particle suspensions, and compare its performance to the explicit Papanastasiou-regularised (PR) two-relaxation-time (TRT) model. In initial 2-D simulations for fluid flow past a single fixed sphere, stability and convergence issues arose in the Newtonian results obtained by the IR model. When extended to Bingham fluids, however, these disappeared, with drag results showing excellent agreement to those in the literature over a range of Bi and Re in the creeping and inertial flow regimes. On the other hand, the TRT model exhibited spurious results, namely viscosity-dependent drag. While the bounce-back cylinder boundary formulation had a small range of stabil-

ity, the dependence of the drag solution on the fluid's viscosity was magnified with the immersed moving boundary formulation. It was concluded that this resulted from a coupling of the ill-defined high viscosity regions present in the Papanastasiou regularisation with the kinetic nature of the LBM-DEM.

An investigation into the vortex shedding characteristics of a Bingham fluid was also conducted, in which it was concluded that the shedding frequency decreased with increasing Bi. For Bi larger than approximately 2.7 - 2.8 vortex shedding did not occur.

The key outcome of the next experiment, which assessed Bingham flow through an array of cylinders, was the successful validation of 2-D inter-particle hydrodynamic effects obtained with the IR model. In particular, the increase in drag at a high porosity reported in the literature study was replicated. However, compared to the PR study, the present IR model obtained significantly lower drags at high Bi, an observation which was attributed to the better accuracy of the implicit solution compared to the Papanastasiou regularisation of the study for $Bi > 20$.

In assessing the performance of the implicit regularisation in three dimensions, creeping Bingham flow past a fixed sphere was first analysed. An initial grid refinement and domain independence study illustrated a high dependence of the drag in high Bi flow on grid resolution and domain size, the latter of which resulted from the slip walls of the domain. Neither a grid nor domain independent solution was attainable with the available computing memory, presenting a limitation of the IR model pertinent to this investigation. In terms of validation, flow fields obtained with the IR model were shown to capture the significant flow features presented in the literature, bar the formation of solid polar caps, which was suggested to result flow interactions at the slip-walls. Additionally, drag results for creeping flow were shown to compare extremely well to existing numerical studies for $Bi < 50$, above which drag was underestimated due to the lack of grid refinement. Hence, for improved literature comparison for future studies, it is recommended that moving test cell walls are implemented to remove slip-wall effects. Dependence of the TRT model solution on viscosity was still present for the 3-D scenario, yet to a much lesser extent than the 2-D simulations. The creeping drag results matched those of IR model, albeit consistently slightly underestimated, which was suggested as an outcome of the explicit regularisation.

Moving on to the problem of a moving particle, the IR model exactly predicted, in relation to numerical literature results, the critical yield-stress at which the gravitational force overcame the opposing yield force. The TRT model, however, exhibited over-yielding of the fluid, overestimating the critical yield-stress. Letting the sphere settle, the terminal drag force observed by the IR model over a range of creeping and inertial flows exhibited excellent correlation to literature results, confirming the correct modelling of inertial, viscous and yield-stress effects. While the TRT model also exhibited good correlation

for creeping flows, the drag was significantly underestimated compared to the literature results for higher Re. This was the final illustration of the superior robustness of the IR model compared to that of the TRT model.

As a final validation metric of the IR model, the hydrodynamic interactions between two co-linear spheres were analysed. As in the literature, sphere interaction effects decreased with increasing Bi. The variation of the un-yielded regions surrounding the spheres also matched those in the literature.

Based on the findings presented, it can be concluded that the aim of the investigation, to assess and compare the performance of an implicitly-regularised model for the potential modelling of viscoplastic particle suspensions to current explicitly-regularised models, was fulfilled. From this evaluation, the present IR LBM-DEM model was shown to perform extremely well in viscoplastic fluid-particle coupling. Additionally, the hypothesis that the implicit regularisation was superior to the Papanastasiou regularisation was confirmed. Significantly, the IR model has been confirmed as an accurate and viable method for the direct numerical simulation of dense viscoplastic particle suspensions. Additionally, validation of the implicit modelling approach affords implementation to a number of other non-Newtonian fluid models, such as the shear thinning and thickening Herschel-Bulkley model.

References

[1] R.P. Chhabra. *Bubbles, Drops, and Particles in Non-Newtonian Fluids*. CRC Press, 2006.

[2] Steph R. Connors, Joseph S. Hezir, Gregory S. Mcrae, Harvey Michaels, and Carolyn Ruppel. The future of natural gas. Technical report, Massachusetts Institute of Technology, 2010.

[3] J. Adachi, E. Siebrits, A. Peirce, and J. Desroches. Computer simulation of hydraulic fractures. *International Journal of Rock Mechanics and Mining Sciences*, 2007.

[4] Carl Montgomery. *Effective and Sustainable Hydraulic Fracturing*. INTECH, 2013.

[5] K. B. Hill and C. A. Shook. Pipeline transport of coarse particles by water and by fluids with yield stress. *Particulate Science and Technology*, 16(2):163–183, 1998.

[6] Eugene C. Bingham. An investigation of the laws of plastic flow. *Bulletin of the Bureau of Standards*, 13:309–353, 1916.

[7] A. Vikhansky. Lattice-boltzmann method for yield-stress liquids. *Journal of Non-Newtonian Fluid Mechanics*, 155(3):95 – 100, 2008.

[8] E.J. ODonovan and R.I. Tanner. Numerical study of the bingham squeeze film problem. *Journal of Non-Newtonian Fluid Mechanics*, 1984.

[9] Tasos C. Papanastasiou. Flows of materials with yield. *Journal of Rheology*, 31(5):385–404, 1987.

[10] A. N. Beris, J. A. Tsamopoulos, R.C. Armstrong, and R.A. Brown. Creeping motion of a sphere through a bingham plastic. *Journal of Fluid Mechanics*, 1985.

[11] J. Blackery and E. Mitsoulis. Creeping motion of a sphere in tubes filled with a bingham plastic material. *Journal of Non-Newtonian Fluid Mechanics*, 70:59–77, 1997.

[12] Benjamin T Liu, Susan J Muller, and Morton M Denn. Convergence of a regularization method for creeping flow of a bingham material about a rigid sphere. *Journal of Non-Newtonian Fluid Mechanics*, 102(2):179 – 191, 2002. A Collection of Papers

Dedicated to Professor {ANDREAS} {ACRIVOS} on the Occasion of his Retirement from the Benjamin Levich Institute for Physiochemical Hydrodynamics and the City College of the {CUNY}.

[13] W. Regulski, C. R. Leonardi, and J. Szumbarski. On the spatial convergence and transient behavior of lattice boltzmann methods for modeling fluids with yield stress. *Preprint submitted to Journal of Computational Physics*, 2016.

[14] D. J. Tritton. Experiments on the flow past a circular cylinder at low reynolds numbers. *Journal of Fluid Mechanics*, 6(4):547 – 567, November 1959.

[15] N. Nirmalkar and R.P. Chhabra. Momentum and heat transfer from a heated circular cylinder in bingham plastic fluids. *International Journal of Heat and Mass Transfer*, 70:564 – 577, 2014.

[16] P. D. M. Spelt, A. Y. Yeow, C. J. Lawrence, and T. Selerland. Creeping flow of bingham fluids through arrays of aligned cylinders. *Journal of Non-Newtonian Fluid Mechanics*, 129(2):66–74, 2005.

[17] Prashant and J.J. Derksen. Direct simulations of spherical particle motion in bingham liquids. *Computers & Chemical Engineering*, 35(7):1200 – 1214, 2011.

[18] Song-Gui Chen, Chuan-Hu Zhang, Yun-Tian Feng, Qi-Cheng Sun, and Feng Jin. Three-dimensional simulations of bingham plastic flows with the multiple-relaxation-time lattice boltzmann model. *Engineering Applications of Computational Fluid Mechanics*, 10:347–360, 2016.

[19] J.P. du Plessis and R.W. Ansley. Settling parameters in solids pipelining. *Journal of the Pipeline Division*, 1967.

[20] N. Nirmalkar, R. P. Chhabra, and R. J. Poole. Numerical predictions of momentum and heat transfer characteristics from a heated sphere in yield-stress fluids. *Industrial & Engineering Chemistry Research*, 52(20):6848–6861, 2013.

[21] R.W. Ansley and T.N. Smith. Motion of spherical particles in a bingham plastic. *AIChE Journal*, 1967.

[22] D.D. Atapattu, R.P. Chhabra, and P.H.T. Uhlherr. Creeping sphere motion in herschel-bulkley fluids: flow field and drag. *Journal of Non-Newtonian Fluid Mechanics*, 59(23):245 – 265, 1995.

[23] L. Valentik and R.L. Whitmore. The terminal velocity of spheres in bingham plastics. *British Journal of Applied Physics*, 1965.

[24] H Pazwash and J Robertson. Forces on bodies in bingham fluids. *Journal of Hydraulic Research*, 13:35–55, 1975.

[25] H.a Tabuteau, P.a b Coussot, and J.R.a De Bruyn. Drag force on a sphere in steady motion through a yield-stress fluid. *Journal of Rheology*, 51(1):125–137, 2007. cited By 58.

[26] Benjamin T. Liu, Susan J. Muller, and Morton M. Denn. Interactions of two rigid spheres translating collinearly in creeping flow in a bingham material. *Journal of Non-Newtonian Fluid Mechanics*, 113(1):49 – 67, 2003.

[27] Zhaosheng Yu and Anthony Wachs. A fictitious domain method for dynamic simulation of particle sedimentation in bingham fluids. *Journal of Non-Newtonian Fluid Mechanics*, 145(23):78 – 91, 2007.

[28] Bruce D. Jones, Christopher R Leonardi, John R Williams, and S.D.R. Others. Validation of a numerical framework for simulation of dense particle suspensions. *Journal of Fluid Mechanics*, 2015.

[29] C. Ancey and H. Jorrot. Yield stress for particle suspensions within a clay dispersion. *Journal of Rheology*, 45:297–319, 2001.

[30] F. Mahaut, X. Chateau, P. Coussot, and G. Ovarlez. Yield stress and elastic modulus of suspensions of noncolloidal particles in yield stress fluids. *Journal of Rheology*, 52:287, 2008.

[31] Xavier Chateau, Guillaume Ovarlez, and Kien Luu Trung. Homogenization approach to the behavior of suspensions of noncolloidal particles in yield stress fluids. *Journal of Rheology*, 52(2):489–506, 2008.

[32] Simon Dagois-Bohy, Sarah Hormozi, lisabeth Guazzelli, and Olivier Pouliquen. Rheology of dense suspensions of non-colloidal spheres in yield-stress fluids. *Journal of Fluid Mechanics*, 776, 2015.

[33] Cyrus K. Aidun and Jonathan R. Clausen. Lattice-boltzmann method for complex flows. *Annual Review of Fluid Mechanics*, 2009.

[34] Martin Geier, Martin Schnherr, Andrea Pasquali, and Manfred Krafczyk. The cumulant lattice boltzmann equation in three dimensions: Theory and validation. *Computers & Mathematics with Applications*, 70(4):507 – 547, 2015.

[35] Song-Gui Chen, QiCheng Sun, Fen Jin, and JianGuo Liu. Simulations of bingham plastic flows with the multiple-relaxation-time lattice boltzmann model. *Sci China-Phys Mech Astron*, 57:532–540, 2014.

[36] Dominique d'Humieres and Irina Ginzburg. Viscosity independent numerical errors for lattice boltzmann models: From recurrence equations to "magic" collision numbers. *Computers & Mathematics with Applications*, 58(5):823 – 840, 2009. Mesoscopic Methods in Engineering and Science.

[37] Stefan Luding. *Dicrete Modelling of Goematerials*, chapter Introduction to Discrete Element Methods: Basics of Contact Force Models and how to perform te Micro-Macro Transission to Continuum Theory, pages 785–826. Multi Scale Mechanics, TS, CTW, UTwente, P.O.Box 217, 7500 AE Enschede, Netherlands, 2008.

[38] J. R. Williams and R. O'Connor. Discrete element simulation and the contact problem. *Archives of Computational Methods in Engineering*, 1999.

[39] B. K. Cook, D. R. Noble, and J. R. Williams. A direct simulation method for particle-fluid systems. *Engineering Computations*, 2004.

[40] C. R. Leonardi, D. R. J. Owen, and Y. T. Feng. Simulation of fines migration using a non-newtonian lattice boltzmann-discrete element model. *Engineering Computations*, 29(4):392–418, 2012.

[41] Yuanxun Bill Bao and Justin Meskas. Lattice boltzmann method for fluid simulations. http://www.cims.nyu.edu/ billbao/report930.pdf, April 14 2011.

[42] D. R. Noble and J. R. Torczynski. A lattice-boltzmann method for partially saturated computational cells. *International Journal of Modern Physics C*, 09(08):1189–1201, 1998.